RAS isoform specific activities are disrupted by disease associated mutations during cell differentiation

Rohan Chippalkatti[1a], Bianca Parisi[1a], Farah Kouzi[1], Christina Laurini[1], Nesrine Ben Fredj[1] and Daniel Kwaku Abankwa[1*]

[1]Cancer Cell Biology and Drug Discovery group, Department of Life Sciences and Medicine, University of Luxembourg, 4362, Esch-sur-Alzette, Luxembourg

[a] these authors contributed equally

[*]correspondence: daniel.abankwa@uni.lu

Abstract

The Ras-MAPK pathway is aberrantly regulated in cancer and developmental diseases called RASopathies. While typically the impact of Ras on the proliferation of various cancer cell lines is assessed, it is poorly established how Ras affects cellular differentiation.

Here we implement the C2C12 myoblast cell line to systematically study the effect of Ras mutants and Ras-pathway drugs on differentiation. We first provide evidence that a minor pool of Pax7+ progenitors replenishes a major pool of transit amplifying cells that are ready to differentiate. Our data indicate that Ras isoforms have distinct roles in the differentiating culture, where K-Ras is more important than N-Ras to maintain the progenitor pool and H-Ras is significant for terminal differentiation. This assay could therefore provide significant new insights into Ras biology and Ras-driven diseases.

In line with this, we found that all oncogenic Ras mutants block terminal differentiation of transit amplifying cells. Notably, while RASopathy K-Ras variants that are also NF1-GAP resistant also block differentiation, albeit less than their oncogenic counterparts. Profiling of targeted Ras-pathway drugs on oncogenic Ras mutants revealed their distinct abilities to restore normal differentiation as compared to triggering cell death. In particular, the MEK-inhibitor trametinib could broadly restore differentiation, while the mTOR-inhibitor rapamycin broadly suppressed differentiation.

We expect that this quantitative assessment of the impact of Ras-pathway mutants and drugs on cellular differentiation has great potential to complement cancer cell proliferation data.

Key words: Ras; cancer; RASopathy; C2C12; flow cytometry; inhibitors; differentiation

Introduction

Malignant tumors are characterized by abnormal proliferation and invasive growth of dedifferentiated tissue. The Ras-pathway is central to control cellular proliferation, differentiation and survival, and is dysregulated in virtually every cancer (Crespo & Leon, 2000; Hanahan, 2022). Three *RAS* genes, *KRAS*, *NRAS* and *HRAS,* are mutated in 19 % of human cancers making *RAS* the most frequently mutated oncogene (Prior *et al*, 2020). Out of the two *KRAS* splice isoforms, K-Ras4A and K-Ras4B, the latter is the highest expressed

51 isoform and the major focus of current drug development (Hood *et al*, 2023; Moore *et al*, 2020;
52 Tsai *et al*, 2015).
53 Ras membrane association is required for its activity, and membrane affinity is mediated by C-
54 terminal lipid modifications of Ras by farnesyltransferase and palmitoyltransferases (Pavic *et*
55 *al*, 2022). Farnesylation also mediates binding of Ras to trafficking chaperones, such as PDE6D
56 and calmodulin, which facilitate its diffusion, followed by trapping on secretory organelles,
57 and subsequent vesicular transport to the plasma membrane (Schmick *et al*, 2015).
58 Canonical Ras signaling emerges at the plasma membrane, where extracellular mitogens
59 activate receptor tyrosine kinases, such as epidermal growth factor receptor (EGFR), which
60 indirectly relays its activation to guanine nucleotide exchange factors (GEFs), such as SOS.
61 GEFs facilitate exchange of GDP for GTP, thus activating Ras. The active GTP-bound Ras
62 then recruits effector proteins, such as Raf, PI3K and RalGDS from the cytosol to the
63 membrane, leading to their activation (Simanshu *et al*, 2017). Raf-kinases trigger the MAPK-
64 pathway, which includes activation of downstream kinases MEK and ERK, the latter of which
65 leads to well characterized changes that drive the cell cycle and thus proliferation (Crespo &
66 Leon, 2000). The effector PI3K activates the kinase Akt, which further downstream engages
67 the mTORC1-pathway and thus cell growth and many other crucial cellular processes
68 (Laplante & Sabatini, 2013). Ras can furthermore activate mTORC2, which phosphorylates
69 Akt on Ser473 (Kovalski *et al*, 2019).
70 The active state of Ras is tightly regulated, with GTP-Ras becoming inactivated by GTPase-
71 activating proteins (GAPs) (Simanshu *et al.*, 2017). The most prominently studied GAP is
72 neurofibromin 1 (NF1), which is recruited aided by B-Raf and one of three SPRED proteins to
73 K-Ras nanodomains of the plasma membrane (Siljamaki & Abankwa, 2016; Stowe *et al*, 2012;
74 Yan *et al*, 2020). Landmark structural data from the mid 1990s already explained how hotspot
75 oncogenic mutations in codons 12 and 61 of Ras disable the GTP-hydrolysis of Ras by NF1
76 and other arginine-finger GAPs (Ahmadian *et al*, 1997; Scheffzek *et al*, 1997). However, the
77 heterotrimeric G protein GAP RGS3 with a catalytic asparagine, was recently shown to
78 facilitate GTP-hydrolysis of all major oncogenic K-Ras mutants (G12D/V, G13C/D) (Li *et al*,
79 2021), suggesting that a distinct function of NF1 is disabled by oncogenic Ras.
80
81 In line with the mitogen-independent mutational activation of Ras, cancer cell assays typically
82 assess the uncontrolled cell growth. Proliferation assays provided a wealth of data in cancer
83 research, such as from large scale genetic and chemical screens (Barretina *et al*, 2012;
84 McDonald *et al*, 2017; Tsherniak *et al*, 2017). However, among pathologists it is well

85 established that dedifferentiation is the most unsettling hallmark of cancer (Chaffer &
86 Weinberg, 2015; Hanahan, 2022). Unfortunately, the functions of Ras during cellular
87 differentiation are only poorly understood and typically not assayed.
88 This lack of understanding also impacts on the treatment development for another type of Ras-
89 driven diseases. Germline mutations in the RAS-MAPK pathway lead to individually rare but
90 collectively common developmental syndromes called RASopathies, which are characterized
91 by facial malformations, short stature, cutaneous defects, cardiac hypertrophy and a pre-
92 disposition to cancer (Castel *et al*, 2020; Rauen, 2013). They illustrate how even a mild
93 overactivation of the MAPK-pathway during embryonal development perturbs proper
94 differentiation in multiple organ systems.
95 For instance, the RASopathy Noonan syndrome can be caused by the *KRAS-D153V* mutation,
96 which in contrast to cancer-associated hotspot mutations, is still sensitive to the GAP NF1, but
97 shows mildly increased effector binding (Gremer *et al*, 2011). Loss-of-function mutations in
98 *NF1* itself lead to neurofibromatosis type I, one of the more common RASopathies (Rauen,
99 2013). This disorder shares some phenotypic similarities with the very rare RASopathy Legius
100 syndrome, which is caused by heterozygous loss-of-function mutations in the *SPRED1* gene
101 (Brems *et al*, 2012). To analyze RASopathy mutants, dedicated low-throughput assays have
102 been developed, which characterize early developmental defects during gastrulation or later in
103 the whole organism in zebrafish and mouse animal models (Jindal *et al*, 2015). Yet, insufficient
104 developmental or cell differentiation assay capacities may underlie the lack of efficacious
105 therapies for most RASopathies (Gross *et al*, 2020).
106 These observed developmental defects in RASopathies are consistent with the deep integration
107 of MAPK-signaling already at the level of stem cell maintenance. During organismal
108 development, pluripotent stem cells give rise to a vast variety of differentiated tissues
109 (Morrison & Kimble, 2006). Both during priming of naïve mouse embryonic stem cells and
110 maintenance of pluripotency in human induced pluripotent stem cells is the MAPK-pathway
111 involved (Altshuler *et al*, 2018; Haghighi *et al*, 2018). In the fully developed organism, adult
112 stem and progenitor cells are important for tissue homeostasis. They typically divide
113 asymmetrically, giving rise to one stem cell (referred to as self-renewal) and one committed or
114 differentiated cell (Morrison & Kimble, 2006).
115 The C2C12 cell model is one of the best characterized *in vitro* differentiation systems, which
116 recapitulates essential *in vivo* processes (Yin *et al*, 2013). This cell line was derived from a
117 skeletal muscle of a 2-month old mouse, and is typically considered a heterogenous population
118 of myoblasts (myogenic progenitor cells), which proliferate and remain undifferentiated under

119 high serum conditions (Bennett & Tonks, 1997). Mitogen withdrawal in low serum culture
120 conditions, rapidly triggers terminal differentiation of the majority of C2C12 cells into
121 multinucleated myotubes within five days (Bennett & Tonks, 1997).
122 However, it is known that a small fraction of proliferating C2C12 cells expresses the muscle
123 progenitor marker Pax7, a paired box transcription factor, as well as the basic helix-loop-helix
124 transcription factor Myf5 (Yoshida *et al*, 1998). Differentiating cells downregulate Pax7 and
125 upregulate myogenic factors, such as MyoD, myogenin and subsequently late differentiation
126 markers, such as the motor protein myosin II heavy chain (MyHC) (Brown *et al*, 2012; Olguin
127 & Olwin, 2004). Interestingly, upon serum withdrawal a minor fraction remains
128 undifferentiated and continues to express the progenitor marker Pax7, but no MyoD, Myf-5 or
129 myogenin (Olguin & Olwin, 2004; Yoshida *et al.*, 1998). These features strikingly resemble
130 quiescent satellite cells, the Pax7 positive adult stem cell population in muscles (Yablonka-
131 Reuveni & Rivera, 1994). Currently, it is not fully resolved, how the minor fraction of myoblast
132 progenitors is connected to a major fraction of differentiated cells.
133 Myogenic differentiation is initiated by a rapid upregulation of SPRED1 upon serum switching
134 and a subsequent decrease in MAPK-signaling (Bennett & Tonks, 1997; Wakioka *et al*, 2001).
135 In line with mitogens maintaining proliferation of myoblasts, oncogenic Ras prevents
136 myogenic differentiation by downregulating the myogenic transcription factor MyoD and
137 myogenin (Lassar *et al*, 1989). Conversely, overexpression of tumor suppressors, such as
138 Sprouty2 and SPRED1 stimulate myogenesis even under high serum conditions (de Alvaro *et*
139 *al*, 2005; Wakioka *et al.*, 2001). Terminal differentiation is then promoted by mTORC2-Akt
140 activity (Shu & Houghton, 2009).
141
142 The proper differentiation trajectories of tissues is perturbed in cancer and may lead to the
143 emergence of rare cancer stem cells, which alone have the potential to seed new tumors, for
144 example during metastization and relapse after therapy (Morrison & Kimble, 2006). Current
145 cancer stem cell models suggest either reprogramming of differentiated cells or an evolution
146 directly from transformed stem/ progenitor cells (Ansieau, 2013; Batlle & Clevers, 2017).
147 Cancer stem cells are best characterized in functional and lineage tracing assays *in vivo* (Nassar
148 & Blanpain, 2016). Yet, *in vitro* surrogate assays persist, such as flow cytometry based
149 detection of cancer stem cell markers (e.g., CD44+/CD24-), or of cancer stem cells in the side
150 population, which is characterized by their increased drug efflux properties (Golebiewska *et*
151 *al*, 2011; Li *et al*, 2017). In addition, low serum, non-adherent 3D spheroid cultures of human
152 mammary stem/ progenitors cells, called mammospheres, were originally employed to

153 maintain and study such cells in culture (Dontu *et al*, 2003). Subsequently these culture
154 conditions were widely adopted to monitor cancer cell stemness from tumorospheres
155 (Weiswald *et al*, 2015). The simplicity of this assay enabled screening for compounds that may
156 have a potential to target specifically cancer stem cells (2022; Mathews *et al*, 2012; She *et al*,
157 2021).
158
159 Current data suggest that *KRAS* is the strongest driver of stemness features, followed by *NRAS*
160 and *HRAS* (Najumudeen *et al*, 2016; Quinlan *et al*, 2008; Wang *et al*, 2015). This potency order
161 that was obtained across multiple model systems strikingly correlates with the *RAS* mutation
162 frequency in cancer (Chippalkatti & Abankwa, 2021). Salinomycin was one of the first cancer
163 stem cell selective inhibitors that was described by the Weinberg group (Gupta *et al*, 2009).
164 This and related compounds showed selective activity against K-Ras, but not H-Ras,
165 suggesting that K-Ras is of high significance in cancer stem cells (Najumudeen *et al.*, 2016;
166 Okutachi *et al*, 2021; Siddiqui *et al*, 2021). While these natural products may become starting
167 points for the development of more potent drugs, they contrast with dedicated inhibitors raised
168 against the target K-Ras. Two such inhibitors, sotorasib (AMG 510) and adagrasib (MRTX849)
169 have recently been approved (Canon *et al*, 2019; Fell *et al*, 2020). Essentially all of these
170 covalent K-Ras-G12C specific inhibitors were built on the development of the compound ARS-
171 1620 (Janes *et al*, 2018). Moreover, MRTX849 derivatives gave rise to other non-covalent
172 inhibitors, including MRTX1133 against K-Ras-G12D (Wang *et al*, 2022). While allele
173 specific inhibitors promise uniquely small side-effects, their limited applicability necessitates
174 the development of innovative K-Ras inhibitors with new modes of action (Steffen *et al*, 2023).
175
176 Here we utilized mainly flow cytometry-based differentiation marker quantification to
177 understand the impact of the three Ras isoforms, notably K-Ras4B, on C2C12 cell
178 differentiation. We first establish a new baseline of understanding C2C12 cell differentiation,
179 by elaborating that Pax7+ progenitors replenish a major pool of Pax7- transit amplifying cells,
180 which then give rise to the MyHC+ differentiated cells.
181 We then elaborate the distinct impact of Ras isoforms on differentiation using specific genetic
182 perturbations. Finally, we demonstrate the applicability of our assay for medium throughput
183 assessment of Ras-pathway drugs to restore differentiation that was perturbed by disease-
184 associated Ras-isoforms and -alleles. Our results demonstrate how profoundly Ras-isoforms
185 impact on cell differentiation and demonstrate how to rapidly analyze the effect of Ras-mutants
186 and -drugs on differentiation.

187 **STAR Methods**

188 Key resources table

189

REAGENT or RESOURCE	SOURCE	IDENTIFIER
Antibodies		
Mouse monoclonal anti-Pax7 (Pax7); dilution 1:100 flow cytometry (FC)	Bio-Techne	Cat# MAB1675 RRID: AB_2159833
Mouse monoclonal anti-myogenin (5FD); dilution 1:100 FC; dilution 1:500 Western blotting (WB)	ThermoFisher Scientific	Cat# 14-5643-82 RRID: AB_1907431
Mouse monoclonal anti-Myosin 4 (MF20), eFluor 660; dilution 1:100 FC	ThermoFisher Scientific	Cat# 50-6503-82 RRID: AB_2574267
Mouse monoclonal anti-Myosin 4 (MF20); dilution 1:100 FC	ThermoFisher Scientific	Cat# 14-6503-82 RRID: AB_2572894
Mouse monoclonal anti-Pax7, Alexa Fluor 488 (Pax7); dilution 1:25 FC	Santa Cruz Biotechnology	Cat# sc81648 RRID: AB_2159836
Mouse monoclonal anti-Histone H3 phospho (Ser10), Alexa fluor 647 (11D8); dilution 1:20 FC	BioLegend	Cat# 650805 RRID: AB_2564361
Mouse monoclonal anti-GAPDH, (GAPDH-71.1); dilution 1:10,000 WB	Merck	Cat# G8795 RRID: AB_1078991
Rabbit polyclonal anti-GAPDH; dilution 1:10,000 WB	Merck	Cat# G9545 RRID: AB_796208
Mouse monoclonal anti-Pax7 (Pax7); dilution 1:500 WB	Santa Cruz Biotechnology	Cat# sc-81648 RRID: AB_2159836
Rabbit polyclonal anti-MYH1 (N-terminal); dilution 1:500 WB	Proteintech	Cat# 25182-1-AP RRID: AB_2879947
Rabbit polyclonal anti-p44/42 MAPK (ERK1/2); dilution 1:1000 WB	Cell Signaling Technology	Cat# 9102 RRID: AB_330744
Mouse monoclonal anti-phopsho-p44/42 MAPK (ERK1/2) (Thr202/Tyr 204) (E10); dilution 1:2000 WB	Cell Signaling Technology	Cat# 9106 RRID: AB_331768
Mouse monoclonal anti-Akt (pan) (40D4); dilution 1:2000 WB	Cell Signaling Technology	Cat# 2920 RRID: AB_1147620
Rabbit monoclonal anti-phospho-Akt (Ser473) (D9E); dilution 1:1000 WB	Cell Signaling Technology	Cat# 4060 RRID: AB_2315049
Mouse monoclonal anti-KRAS (3B10-F2); dilution 1:1000 WB	Merck	Cat# WH0003845M1 RRID: AB_1842235
Rabbit polyclonal anti-HRAS; dilution 1:1000 WB	Proteintech	Cat# 18295-1-AP RRID: AB_2121046

Mouse monoclonal anti-NRAS (F155); dilution 1:1000 WB (dilution 1:250 for si*HRAS*)	Santa Cruz Biotechnology	Cat# sc-31 RRID: AB_628041
IRDye 680RD goat anti-Rabbit IgG; dilution 1:10,000 WB	LI-COR Biosciences	Cat# 926-68071 RRID: AB_10956166
IRDye 680LT donkey anti-Mouse IgG; dilution 1:10,000 WB	LI-COR Biosciences	Cat# 926-68022 RRID: AB_10715072
IRDye 800CW goat anti-Rabbit IgG; dilution 1:10,000 WB	LI-COR Biosciences	Cat# 926-32211 RRID: AB_621843
IRDye 800CW donkey anti-Mouse IgG; dilution 1:10,000 WB	LI-COR Biosciences	Cat# 926-32212 RRID: AB_621847
Bacterial and virus strains		
E. coli DH10B	New England BioLabs	Cat# C3019I
Biological samples		
N/A	N/A	N/A
Chemicals, peptides, and recombinant proteins		
Sotorasib (AMG 510)	MedChem Express	Cat# HY-114277 CAS# 2296729-00-3
ARS-1620	MedChem Express	Cat# HY-U00418 CAS# 1698055-85-4
MRTX1257	MedChem Express	Cat# HY-114436 CAS# 2206736-04-9
MRTX1133	MedChem Express	Cat# HY-134813 CAS# 2621928-55-8
Trametinib	MedChem Express	Cat# HY-10999 CAS# 871700-17-3
Adagrasib (MRTX849)	Selleckchem	Cat# S8884 CAS# 2326521-71-3
Cysmethynil	Cayman Chemical	Cat# 14745 CAS# 851636-83-4
Rapamycin	BioVision	Cat# 1568 CAS# 53123-88-9
Tipifarnib	Selleckchem	Cat# S1453 CAS# 192185-72-1
BI-3406	MedChem Express	Cat# HY-125817 CAS# 2230836-55-0
Gefitinib	Biorbyt	Cat# orb545838 CAS# 184475-35-2
Dimethyl sulfoxide (DMSO)	PanReac AppliChem	Cat# A3672 CAS# 67-68-5
Critical commercial assays		
Gateway LR Clonase II enzyme mix	ThermoFisher Scientific	Cat# 11791020
APC conjugation kit – Lightning-Link	Abcam	Cat# ab201807
PE/R-Phycoerythrin conjugation kit – Lightning Link	Abcam	Cat# ab102918

Cell proliferation staining reagent – Deep Red Fluorescence (Cytopainter deep red)	Abcam	Cat# ab176736
Cell proliferation staining reagent – Orange Fluorescence (Cytopainter orange)	Abcam	Cat# ab176737
Bio-Rad Protein Assay Kit I	Bio-Rad	Cat# 5000001
Pierce Protease Inhibitor Tablets	ThermoFisher Scientific	Cat# A32963
PhosSTOP	Merck	Cat# 4906845001
Lipofectamine RNAiMAX Transfection Reagent	ThermoFisher Scientific	Cat# 13778075
Lipofectamine 2000 Transfection Reagent	ThermoFisher Scientific	Cat# 11668019
TRIzol Reagent	ThermoFisher Scientific	Cat# 15596018
SuperScriptIII Reverse Transcriptase	ThermoFisher Scientific	Cat# 18080093
SsoAdvanced Universal SYBR Green Supermix	Bio-Rad	Cat# 1725274
FITC Annexin V Apoptosis detection kit I	BD Biosciences	Cat# 556547
Experimental models: Cell lines		
Mouse cell line, C2C12	ATCC	Cat# CRL-1772 RRID: CVCL_6974
Experimental models: Organisms/strains		
N/A	N/A	N/A
Oligonucleotides		
Custom qPCR primer: KRAS human_F 5’-3’ sequence TACAGTGCAATGAGGGACCA	Genecust	N/A
Custom qPCR primer: KRAS human_R 5’-3’ sequence TCCTGAGCCTGTTTTGTGTCT	Genecust	N/A
Custom qPCR primer: NRAS mouse_F 5’-3’sequence TAACCTCTACAGGGAGCAAAT	ThermoFisher Scientific	N/A
Custom qPCR primer: NRAS mouse_R 5’-3’ sequence GTTGACACAAAGCAAGCCCAC	ThermoFisher Scientific	N/A
Custom qPCR primer: HRAS mouse_F 5’-3’ sequence AGCAGATCAAGCGGGTGAAA	ThermoFisher Scientific	N/A
Custom qPCR primer: HRAS mouse_R 5’-3’ sequence ATCGGGTGGGTTCAGTTTCC	ThermoFisher Scientific	N/A
Custom qPCR primer: GAPDH mouse_F 5’-3’ sequence TGGTGAAGGTCGGTGTGAA	Eurogentec	N/A
Custom qPCR primer: GAPDH mouse_R 5’-3’ sequence ATGAAGGGGTCGTTGATGG	Eurogentec	N/A
Negative control siRNA	QIAGEN	Cat# 1027310 GeneGlobe ID: SI03650325
Human *HRAS* siRNA (FlexiTube siRNA) 5’-3’sequence CGGAAGCAGGUGGUCAUUA	QIAGEN	Cat# 1027417 GeneGlobe ID: SI02654806

Mouse *KRAS* siRNA (targeting both *KRAS*4A and 4B transcripts) (ON-TARGETplus SMARTpool siRNA) 5'-3' sequences GAACAGUAGACACGAAAA AGCAAGGAGUUACGGGAUU GGUUGGAGCUGGUGGCGUA GGUGUACAGUUAUGUGAAU	Horizon Discovery	Cat# L-043846-01-0005
Custom siRNA: Mouse *NRAS* siRNA 5'-3' sequence GCAAAUUAAGCGUGUGAAAUUU	Horizon Discovery	N/A
Recombinant DNA		
C453-E04: attB4-CMV51p>-attB5	FNL Combinatorial Cloning Platform, RAS-Initiative	Addgene# 162973
pDest-305 (attR4-attR2)	FNL Combinatorial Cloning Platform, RAS-Initiative	Addgene# 161895
C512-E01: attB5r-mEGFP-nostop-attB1r	FNL Combinatorial Cloning Platform, RAS-Initiative	Addgene# 162940
Hs. KRAS4b-WT	RAS mutant collection V2.0, RAS-Initiative	Addgene# 83129
Hs. KRAS4b-G12C	RAS mutant collection V2.0, RAS-Initiative	Addgene# 83130
Hs. KRAS4b-G13D	RAS mutant collection V2.0, RAS-Initiative	Addgene# 83133
Hs. KRAS4b-Q61H	RAS mutant collection V2.0, RAS-Initiative	Addgene# 83140
pDest305-CMV-mEGFP-K-Ras4B WT	This paper	N/A
pDest305-CMV-mEGFP-K-Ras4B G12C	This paper	N/A
pDest305-CMV-mEGFP-K-Ras4B G13D	This paper	N/A
pDest305-CMV-mEGFP-K-Ras4B Q61H	This paper	N/A
pmEGFP-KRas4B-G12V	(Abankwa *et al*, 2010)	N/A
pmEGFP-HRas-G12V	(Abankwa *et al.*, 2010)	N/A
pmEGFP-HA-NRas-G12V	(Abankwa *et al.*, 2010)	N/A
pEGFP-KRAS4B-G12D	(Yelland *et al*, 2022)	N/A
pmEGFP-KRas4B-G12V-S17N	Gene Universal	N/A

pEYFP-wt KRas	(Gremer *et al.*, 2011)	N/A
pEYFP-KRAS4b-T58I	(Gremer *et al.*, 2011)	N/A
pEYFP-KRAS4b-D153V	(Gremer *et al.*, 2011)	N/A
pEYFP-KRAS4b-V14I	(Gremer *et al.*, 2011)	N/A
pEYFP-KRAS4b-P34R	(Gremer *et al.*, 2011)	N/A
pEYFP-KRAS4b-P34L	(Gremer *et al.*, 2011)	N/A
pEYFP-KRAS4b-K5N	(Gremer *et al.*, 2011)	N/A
pEYFP-KRAS4b-K5E	(Gremer *et al.*, 2011)	N/A
pEYFP-KRAS4b-Q22E	(Gremer *et al.*, 2011)	N/A
pEYFP-KRAS4b-G60R	(Gremer *et al.*, 2011)	N/A
pEYFP-KRAS4b-Y71H	(Cirstea *et al*, 2013)	N/A
Software and algorithms		
GuavaSoft version4.0	Cytek Biosciences	N/A
Leica Application Suite X version 4.12	Leica Microsystems	RRID: SCR_013673
GraphPad Prism version 9.5.1	GraphPad	RRID: SCR_002798
Fiji version 2.9.0	Schindelin, 2012	RRID: SCR_002285
FlowFate version 1.2	(Parisi *et al*, 2023)	N/A
Image Studio software version 5.2	LI-COR Biosciences	N/A
Bio-Rad CFX Manager version 3.1	Bio-Rad	N/A
FlowJo version 10 software	FlowJo	N/A
Other		
Guava easyCyte 6HT 2L flow cytometer	Cytek Biosciences	Cat# 0500-4007
Odyssey CLx Infrared Imaging System	LI-COR Biosciences	Cat# LI9140-00
CFX-connect real-time PCR Detection System	Bio-Rad	Cat# 1855200
Dulbecco's Modified Eagle's Medium (DMEM)	ThermoFisher Scientific	Cat# 11965092
Fetal bovine serum (FBS)	ThermoFisher Scientific	Cat# 10270106
Horse serum (HS)	ThermoFisher Scientific	Cat# 16050130
L-glutamine (200 mM)	ThermoFisher Scientific	Cat# A2916801
Penicillin-Streptomycin (10,000 U/mL)	ThermoFisher Scientific	Cat# 10378016
Opti-MEM Reduced Serum Medium	ThermoFisher Scientific	Cat# 31985070
Hank's balanced salt solution (HBSS)	Lonza	Cat# BE10-547F
Paraformaldehyde 16 % (w/v)	Avantor	Cat# 30525-89-4
TWEEN 20	Merck	Cat# P9416
Triton X-100	Merck	Cat# T8787
BsrGI-HF (20,000 U/mL)	New England BioLabs	Cat# R3575S

190

191 Cell Culture and transfections

192 C2C12 cells were maintained in Dulbecco's modified Eagle Medium (DMEM) supplemented
193 with ~9 % (v/v) fetal bovine serum (FBS), 2 mM L-glutamine and 1 % penicillin/streptomycin
194 (high serum culture medium). Cells were incubated in a humidified incubator at 37 °C, with 5
195 % CO_2 and passaged when reaching 50 – 60 % confluency. Passage numbers are indicated in
196 the legends and passages beyond ten were not employed. Cell culture medium was exchanged
197 with DMEM supplemented with ~2 % horse serum (HS), 2 mM L-glutamine and 1 %

198 penicillin/streptomycin (low serum culture medium) to induce differentiation at 90 %
199 confluency. For experiments lasting three to five days fresh DMEM + 2% HS was added every
200 day.
201
202 Preparation of expression constructs
203 Plasmid constructs used for transfection were generated by multisite gateway cloning (Wall *et*
204 *al*, 2014). To generate the final expression constructs, LR Clonase II enzyme mix was used to
205 perform recombination of the entry clones encoding the promoter, the fluorescent tag and the
206 gene of interest with the pDest-305 destination vector. The reaction mix was transformed into
207 ccdB-sensitive *E. coli* strain DH10B. Colonies resistant to ampicillin were selected for
208 screening of their plasmid DNA by restriction digestion with BsrGI-HF enzyme. Plasmids with
209 the expected fragment sizes were then further validated by sequencing. The pmEGFP-KRas4B-
210 G12V-S17N construct was generated by site directed mutagenesis on the pmEGFP-KRas4B-
211 G12V background by Gene Universal (Delaware, USA).
212
213 Plasmid DNA transfection
214 C2C12 cells were seeded in high serum medium at a density of 100,000 cells per mL of a 6-
215 well plate (#10062-892, Avantor) and transfection was performed after the cells reached 50 –
216 60 % confluency (typically 24 h after seeding). Transfection was performed according to the
217 protocols provided by the manufacturer. 2 µg of plasmid DNA and 7.5 µL Lipofectamine 2000
218 were added to 250 µL Opti-MEM medium. The mixture was vortexed, incubated at 22 - 25 °C
219 for 10 min and subsequently added dropwise to one well of a 6-well plate. Medium was
220 exchanged with fresh high serum medium after 4 h. After further 24 h incubation with high
221 serum, medium was exchanged with low serum medium to induce differentiation.
222
223 Knockdown by siRNA transfection
224 Any siRNAs were transfected using Lipofectamine RNAiMAX diluted in Opti-MEM medium.
225 Typically, 100 nM of each siRNA and 7.5 µL of Lipofectamine were added to 250 µL of Opti-
226 MEM medium, mixed and incubated at 22 – 25 °C for 10 min. Cells were transfected at 50 –
227 60 % confluency by adding this mixture. After 24 h of incubation with the siRNA-
228 Lipofectamine mixture, the medium was substituted with fresh high serum medium. After 3 –
229 4 h, high serum medium was exchanged with low serum medium, and cells were cultured in
230 low serum medium that was replaced every day.

231

232 Antibody conjugation with Allophycocyanin (APC) or Phycoerythrin (PE)

233 For flow cytometry experiments anti-Pax7 and anti-myogenin antibodies were conjugated to
234 APC with the reagents provided in the APC conjugation kit – Lightning link. Anti-Myosin 4
235 Monoclonal antibody (anti-MyHC) was conjugated with PE with the components provided in
236 the PE/R-Phycoerythrin conjugation kit – Lightning link. The modifier reagent and quencher
237 reagent were contained in both kits. Additionally, the APC conjugation reaction mix was
238 supplied with the APC kit and the PE conjugation reaction mix was supplied with the PE/R-
239 Phycoerythrin kit. Anti-Pax7 or anti-myogenin antibodies at a concentration of 1 mg/ mL and
240 100 μL volume were mixed with 100 μg APC Conjugation Reaction Mix, together with 10 μL
241 of Modifier Reagent. Similarly, 100 μL of 0.5 mg/mL anti-MyHC antibody was mixed with
242 100 μg PE Conjugation Reaction Mix with 10 μL of Modifier Reagent. This mixture was stored
243 in the dark at 22 – 25 °C for 3 – 4 h. Subsequently, the conjugation reaction was stopped by
244 adding 10 μL quencher reagent to the conjugation mix. The conjugated antibody solution was
245 used at a dilution of 1:100 and stored at 4 °C for up to 6 months.
246 The degree of labelling (DOL) was calculated according to the formula, DOL = (Amax × MW
247 × dilution factor)/(ε × [conjugate]). MW is the molecular weight of IgG (~150,000 g/mol), and
248 ε is the molar extinction coefficient of the dye (e.g. 700,000 M^{-1} cm^{-1} for APC), [conjugate] =
249 {[A280 – (Amax × Cf)]/1.4} × dilution factor. Here, [conjugate] is the concentration in mg/
250 mL of the antibody conjugate, 'dilution factor' is the fold of dilution used for spectral
251 measurements. A280 is the absorbance of the conjugate at 280 nm and Amax is the absorption
252 maximum of APC. Cf is the absorbance correction factor and the value 1.4 is the extinction
253 coefficient of IgG in mg/mL. For APC, Cf is 0.22. We obtained 0.5 – 1 moles of APC per
254 antibody, which falls within the optimal range for labelling. Similar results were obtained with
255 the PE conjugation kit.
256

257 Flow cytometry

258 Cells were seeded at a concentration of 100,000 cells/mL per well of a 6-well plate. This was
259 followed by transfection with the required plasmids or siRNAs and a low serum culture period
260 for the time indicated in the figures or figure legends. Fresh low serum, where required with
261 drug/ compound, was added every day. Cells were then harvested by trypsinization with 0.05
262 % (w/v) trypsin EDTA (1×) for 5 min and pelleted by centrifugation at 500 × g for 5 min. The
263 subsequent steps were performed at 22 - 25 °C. The cell pellet was subsequently fixed with 4

264 % (w/v) paraformaldehyde (PFA) in PBS for 10 min. After washing with PBS, cells were
265 permeabilized with 0.5 % (v/v) Triton X-100 in PBS for 10 min. Subsequently cells were
266 washed with 0.05 % (v/v) Tween 20 in PBS (PBST) and immunolabelled with fluorescent dye-
267 conjugated primary antibodies at the indicated dilutions in PBST for 1 h at 4 °C. Subsequently
268 cells were pelleted by centrifugation at 500 × g for 5 min and resuspended in PBST for flow
269 cytometric analysis.
270 We first gated around 30,000 cells based on their forward and side scatter properties to exclude
271 debris or dead cells. The intact cells thus obtained were further analyzed for expression markers
272 using dot plots. In general, 1,000 to 10,000 EGFP-variant construct expressing intact cells were
273 collected, depending on the treatment condition. Predominantly, mEGFP-tagged constructs
274 were employed, which have the identical brightness as EGFP-tagged constructs (Norris *et al*,
275 2015). EGFP-variants and Alexa Fluor 488 were excited with the 50 mW photodiode 488 nm
276 laser and the fluorescent signal was detected using the Green-B filter (band pass 525/30 nm)
277 on a Guava Luminex easyCyte 6HT 2L flow cytometer. APC or eFluor 660 were excited using
278 the 100 mW photodiode 642 nm laser and detected using the Red-R filter (band pass 661/15
279 nm). PE was excited using the 50 mW photodiode 488 nm laser and detected using the Yel-B
280 filter (band pass 583/26 nm). An unlabeled control sample was always included as a control to
281 correct for autofluorescence. Spectral overlap of PE and EGFP was corrected via digital
282 compensation using single color EGFP-only and PE-only control samples.
283 Labelled or EGFP-variant expressing cells were quantified using the 'Quad Stat plot' feature
284 on the GuavaSoft 4.0 software. The laser power and the voltage gain settings were adjusted
285 such that the unlabeled events appeared below the level of 10^1 relative fluorescence units
286 (RFU). Two EGFP-expression windows were defined, 'GFP low' between 10^1 and 10^2 RFU
287 and 'GFP high' between 10^2 and 10^5 RFU. This allowed to quantitate differentiation in
288 dependence of the EGFP-expression level. The majority of data were analyzed in the GFP low
289 window, which produced a phenotype comparable to non-transfected C2C12 cells. A detailed
290 step-by-step procedure of sample preparation, data acquisition and analysis is described in our
291 previous work (Parisi *et al.*, 2023).
292 To visualize the changes in Pax7+, myogenin+ and MyHC+ cell fractions over time,
293 histograms depicting the fluorescence intensities of marker-labelled populations were
294 generated with the Overlays tool in FlowJo.
295 To evaluate drug-induced cell toxicity, gating was applied based on forward and side scatter
296 characteristics to separate total events into intact cells and debris. The percentage of intact cells

297 among the total events was then plotted for each EGFP-construct and drug treatment to estimate
298 cell toxicity.
299
300 Cell proliferation analysis in dye dilution experiments
301 A 500 × stock solution of Cytopainter deep red/Cytopainter orange was prepared as described
302 by the manufacturer and stored at -20°C. A 1 × working solution was prepared on the day of
303 labelling in Hank's balanced salt solution (HBSS). Cells from a confluent flask were detached
304 with trypsinization, pelleted by centrifugation at 200 × *g* for 3 min and 1 mL high serum
305 medium was added to the pellet. Cells were then counted on a Z1 particle counter (Beckman
306 Coulter) to obtain 100,000 cells per 1 mL high serum medium. Cells were again pelleted by
307 centrifugation at 500 × *g* for 5 min, resuspended in 500 µL cytopainter working solution and
308 incubated in the dark at 37 °C for 15 min. Cells were once more pelleted (500 × *g* for 5 min)
309 and the pellet was washed once with 500 µL HBSS. After another round of pelleting, cells were
310 finally resuspended in 1 mL high serum medium. 200 µL from this cell suspension was kept
311 aside as the day 0 followed by fixation with 4 % (w/v) PFA. Out of the remaining 800 µL, 200
312 µL cell suspension containing 20,000 cells was dispensed per well in 3 wells of a 6-well plate
313 containing 2 mL high serum medium. Cells were then incubated for 3 days in the cell culture
314 incubator. Cells from one well were collected by trypsinization on day 1, day 2 and day 3 and
315 processed for immunofluorescence with mouse monoclonal anti-Pax7, Alexa Fluor 488
316 antibody. Cytopainter deep red fluorescence was detected by 642 nm laser excitation and using
317 the Red-R emission filter (band pass 661/15 nm). The half-life ($t_{1/2}$) of the cytopainter dilution
318 was calculated using the one-phase decay equation in Prism 9.0, Y = (Y0 – plateau) × exp(-K
319 × X) + plateau. Here, X is time (days), Y is the cytopainter mean fluorescence intensity, Y0 is
320 the Y value at day 0 which decays with one phase to plateau and K is the rate constant expressed
321 as a reciprocal of the X axis unit. The $t_{1/2}$ value was calculated as ln(2)/K.
322 The 'Misc parameters' feature on the GuavaSoft software provides the number of events per
323 µL of each sample, which allowed us to calculate the cell concentration per mL of Pax7+ and
324 Pax7- fractions.
325 To analyze cell proliferation in cells transfected with mEGFP-tagged wt K-Ras or K-RasG12V
326 constructs, 100,000 cells/ mL were first seeded in all wells of a 6-well plate. Each construct
327 was transfected in all wells of a 6-well plate. Transfected cells were then harvested by
328 trypsinization, cells from all wells were pooled in a single 15 ml falcon tube and cell
329 concentration was determined with a Z1 particle counter. Cell staining with cytopainter orange

330 reagent was then carried out in exactly as described above for cytopainter deep red. Cells
331 labelled with cytopainter orange were then fixed and immunolabelled with APC conjugated
332 anti-Pax7 antibody. Cytopainter orange fluorescence was detected with 488 nm laser excitation
333 and the Yel-B emission filter (band pass 583/26 nm). Cytopainter orange fluorescence signal
334 for Pax7+ and Pax7- fractions was measured specifically for cells in the 'GFP low' window.
335

336 Cell toxicity analysis with 7-AAD

337 The cell impermeable dye 7-Aminoactinomycin D (7-AAD) is excluded from intact cells but
338 intercalates into the genomic DNA of late apoptotic and necrotic cells since the plasma
339 membrane integrity of these cells is compromised. The toxicity of K-RasG12C inhibitors was
340 analyzed in cell fractions transfected with pDest305-CMV-mEGFP-K-RasG12C. Cells were
341 treated 24 h after transfection with DMSO, sotorasib (AMG 510), MRTX1257 and adagrasib
342 (MTRX849) in low serum for three days at indicated concentrations. The medium was first
343 aspirated from drug treated cells to collect the 'supernatant' fraction of dead cells. The
344 'adherent' fraction of cells was collected by trypsinization. After centrifugation at 500 × *g* for
345 5 min and a washing step with PBS, both fractions were labelled with the provided 7-AAD
346 solution for 15 min on ice according to the manufacturer instructions. The 7-AAD fluorescence
347 was detected using the 100 mW photodiode 642 nm laser and the Red-B filter (band pass
348 635/40 nm) by flow cytometry. Cells expressing EGFP-constructs and labelled with 7-AAD
349 were gated and counted using the Quad Stat plot feature on GuavaSoft software. Percentages
350 of GFP+ 7AAD+ cells were quantified from the GFP low window and plotted for each drug
351 treatment.
352

353 Microscopy

354 Brightfield images were acquired with 10 and 20 × objectives of a Leica DMI3000 B inverted
355 microscope equipped with a Leica DFC360 FX digital camera. Samples were illuminated using
356 pE400max LED white light source from CoolLED. Images were analyzed with Leica LAS X
357 software.
358

359 Immunoblotting

360 Cells were seeded at a density of 100,000 cells/ mL in each well of a 6-well plate, transfected
361 and then cultured in low serum as indicated in the figures. Cells were then washed with ice-
362 cold PBS and lysed for 30 min on ice using a total of 100 µL of lysis buffer (10 mM Tris pH
363 7.5, 150 mM NaCl, 0.5 mM EDTA, 0.2% NP40) supplemented with one tablet of protease

364 inhibitor cocktail per 10 mL lysis buffer. The lysis buffer was additionally supplemented with
365 one tablet per 10 mL of the PhosSTOP phosphatase inhibitor cocktail. Cells were collected
366 using a scraper and incubated on ice for 30 min with intermittent vortexing. Lysates were
367 cleared by centrifugation at 13,000 × *g* for 10 min at 4 °C. Supernatants were collected and
368 quantified by the Bradford assay using Bio-Rad Protein Assay Kit, followed by heating at 95
369 °C for 5 min. Protein samples were then resolved on denaturing SDS-PAGE. A 6 % resolving
370 gel was used for detection of MyHC, 10 % resolving gel for Pax7, ERK1/2, Akt and 15 %
371 resolving gel for detection of myogenin, K-Ras (total K-Ras, both 4A and 4B isoforms), H-
372 Ras, N-Ras. Subsequently, separated proteins were transferred onto a nitrocellulose blotting
373 membrane 0.2 µm by using a TransBlot turbo Transfer System (Bio-Rad). The blots were
374 probed as indicated in the figures with the antibodies diluted as described in the Key Resources
375 Table. The membranes were washed 3 times with PBST (0.2 % (v/v) Tween 20 in PBS) and
376 then incubated with anti-mouse or anti-rabbit IRDye800CW or IRDye680RD/LT conjugated
377 secondary antibodies. Finally, protein bands were detected using a LI-COR ODYSSEY CLx
378 system. Band intensities were quantified using Fiji and normalized to GAPDH. The relative
379 abundances of phosphorylated ERK1/2 and phospho-Akt were quantified as the ratios of the
380 intensities of phosphorylated proteins and the total proteins.
381
382 Quantitative RT-PCR of gene transcripts
383 Cells were seeded at a density of 100,000 cells/ mL of a 6-well plate and transfected with
384 siRNAs directed against *KRAS*, *NRAS* and *HRAS*. Note that the *HRAS* siRNA against the
385 human mRNA was also targeting the identical sequence of the mouse mRNA.
386 After culturing in low serum medium, cells were collected as indicated in the figures. Total
387 RNA was isolated using Trizol according to the manufacturer's protocol. Reverse transcription
388 was performed with 1 µg of total RNA using SuperScriptIII Reverse Transcriptase. The relative
389 abundance of *KRAS*, *NRAS* and *HRAS*, gene transcripts was analyzed by using SsoAdvanced
390 Universal SYBR Green Supermix on the CFX-connect real-time PCR instrument (Bio-Rad)
391 and Bio-Rad CFX Manager Software. Specific amplicons were detected for *KRAS* (both K-
392 Ras4A and K-Ras4B splice variants), *NRAS, HRAS*, and *GAPDH*. Forward and reverse primer
393 sequences *KRAS* and *NRAS* amplicons were described previously (Duggan *et al*, 2019; Tsai *et*
394 *al.*, 2015). Primers for amplification of *HRAS* and *GAPDH* were designed using the online tool
395 'OligoPerfect Primer Designer'. The mRNA sequences of mouse *HRAS* (NM_008284.3) and
396 *GAPDH* (NM_008084.4) were used as templates for primer design. The relative mRNA

397 expression level was calculated using the $2^{-\Delta\Delta Ct}$ method by normalizing to *GAPDH* expression
398 (Livak & Schmittgen, 2001).
399
400 Data and Statistical analysis
401 Prism 9 (GraphPad) was used for the preparation of plots, heatmaps, data and statistical
402 analysis. The number n of analyzed cells that was employed for statistical calculations was at
403 least 2000. These originated from N independent biological repeats as indicated in the figure
404 legends. Bar plots show mean ± SD, if not stated otherwise. Statistical analysis of flow
405 cytometry data was performed by employing the Fisher's Exact test, unless otherwise
406 mentioned in the legends. Immunoblotting data were compared using the unpaired t-test. Half-
407 lives were compared using the Mann-Whitney test.
408 A p-value < 0.05 is considered statistically significant, and the statistical significance levels
409 are annotated as follows: * $p < 0.05$; ** $p < 0.01$; *** $p < 0.001$; **** $p < 0.0001$.
410
411
412 **Results**
413 **Benchmarking of flow cytometry-based analysis of C2C12 differentiation**
414 Differentiation stage-specific markers of mouse muscle C2C12 cells correlate with those
415 identified during muscle development *in vivo* (***Figure 1A***) (Yin *et al.*, 2013). Both the MAPK-
416 and PI3K-pathways downstream of Ras are characteristically regulated during differentiation
417 (Bennett & Tonks, 1997; Wakioka *et al.*, 2001; Xu & Wu, 2000). The C2C12 model therefore
418 offers the opportunity to study the impact of Ras-pathway disease variants and targeted drug
419 treatments on cellular differentiation.
420 We first benchmarked this assay against conventional phenotypic and immunoblotting-based
421 differentiation analysis. C2C12 cell myoblasts assume a roundish-rhomboid morphology when
422 cultured in high serum (day 0) (***Figure 1B***). Medium switching to low serum induces
423 differentiation (day 1), which alters the morphology of cells to become increasingly more
424 spindle shaped. From day 2 to day 3 after serum switching the number of spindle shaped cells
425 visibly increased, and further elongation with subsequent fusion resulted in a robust myotube
426 assembly at day 5 (***Figure 1B***). While determining the fraction of nuclei incorporated into
427 myotubes can measure the overall progression of differentiation as the fusion index, this and
428 related methods are quite tedious and allow only for the analysis of small cell numbers (Velica
429 & Bunce, 2011).

430 In addition, muscle progenitor and differentiation markers are commonly analyzed using
431 immunoblotting, which however captures only the averaged response across the heterogenous,
432 differentiating cell pool. This became obvious when we compared immunoblotting- and flow
433 cytometry-derived results of various muscle differentiation markers during the 5-day
434 differentiation period. Immunoblotting revealed a nearly constant Pax7 protein expression
435 (***Figure 1C***), which were matched by an almost constant fraction of Pax7 positive (Pax7+) cells
436 that exhibited a constant mean Pax7 intensity in the flow cytometry-based analysis (***Figure***
437 ***1D***). By contrast, analysis of the early differentiation marker myogenin by immunoblotting
438 suggested a linear increase of the muscle-specific transcription factor during differentiation
439 (***Figure 1E***). This increase is however not due to an increased number of myogenin positive
440 cells, but an increased mean expression level of the transcription factor in the population, as
441 revealed by the flow cytometry data (***Figure 1F***). Both immunoblotting (***Figure 1G***) and flow
442 cytometric analysis (***Figure 1H***) confirmed that the expression of the late differentiation
443 marker myosin heavy chain (MyHC) rapidly increased between days 2 and 3. In this case both
444 the fraction of MyHC+ cells and the mean expression level in the population increased (***Figure***
445 ***1H***). The flow cytometry-based analysis of C2C12 cell differentiation therefore resolves
446 population level differences in the expression of differentiation markers that may remain
447 hidden in other common types of differentiation analyses. We therefore recently established a
448 protocol to measure C2C12 cell differentiation using the flow cytometric quantification of the
449 MyHC+ fraction, which we furthermore automated by our custom R-script software FlowFate
450 (Parisi *et al.*, 2023).
451 The sensitivity of this assay furthermore enabled us to detect a decline in the differentiation
452 potential with an increase in passage number. Cells with the passage number six (***Figure 1G,H***)
453 arrived at ~20 % MyHC+ cells at day 3, while this fraction declined to ~15 % in passage eight
454 and slightly further to ~13 % in passage ten (***Figure1 – figure supplement 1 A-D***). At the same
455 time, the number of differentiated cells at day 0 in high serum increased in the same order,
456 suggesting that a leakage into differentiation occurs due to passaging even in high serum. As
457 this reduced the net change of the fraction of differentiated cells, i.e. the dynamic range of this
458 assay, we aimed at employing cells with passage numbers from six to nine and included internal
459 references wherever possible. Nevertheless, a residual background fluctuation inherent to
460 variations caused by the passage numbers can be observed in our data that were composed from
461 independent biological repeats across a longer time span.
462

463 **Differentiated cells arise from the major pool of Pax7-/ MyHC- transit amplifying cells**
464 Our analysis revealed that the muscle progenitor marker Pax7 is expressed by a minor sub-
465 population of C2C12 cells (< 1%) before and after induction of differentiation (***Figure 2A***). It
466 is therefore impossible that this population of myoblasts provides the bulk of differentiated
467 Pax7-/ MyHC+ myotubes. Instead, double labelling revealed that concomitant with the
468 increase of the Pax7-/ MyHC+ differentiated cells, a Pax7-/ MyHC- subpopulation decreased
469 that constitutes the bulk of the C2C12 cell line (***Figure 2A***). This strongly suggests that the
470 MyHC+ differentiated cells arise from the Pax7-/ MyHC- cells.
471 To understand how this large pool of Pax7-/ MyHC- cells is maintained under high serum
472 conditions, we analyzed the proliferation of the Pax7+ and Pax7- populations by co-labelling
473 Ser10-phosphorylated histone H3 (pH3), a marker of mitotic and proliferative activity (Goto
474 *et al*, 1999). While ~22 % of Pax7+ myoblasts were also pH3+ at day 0 in high serum, only ~5
475 % of Pax7- cells were pH3+, suggesting that these latter cells have a low mitotic activity. After
476 switching to low serum, the fraction of mitotically active Pax7+ cells dropped to ~12 % (***Figure***
477 ***2B***), while the Pax7- population almost stopped dividing (***Figure 2C***).
478 The higher proliferation rate of Pax7+ cells in high serum was further supported by dye-dilution
479 experiments. The non-toxic cytopainter dye is diluted ~2-fold during each cell division, which
480 was reflected by the decrease in the geometric means of fluorescence intensities in an
481 exponentially growing cell population (***Figure 2D,E***). When cultured under high serum, the
482 cytopainter labelling decayed at a comparable rate in both Pax7+ and Pax7- subpopulations
483 (***Figure 2E***). At the same time, the number of Pax7- cells increased exponentially during the
484 3-day culture in high serum, while that of Pax7+ cells only marginally increased (***Figure 2F***).
485 This proliferation pattern is reminiscent of other developmental systems where a minor pool of
486 progenitors asymmetrically divides to generate one progenitor and one transit amplifying cell.
487 The latter then expand exponentially, while the progenitor pool is preserved (Chia *et al*, 2008).
488 This setup is not only critical during development but also for tissue homeostasis and
489 regeneration in the adult (Gomez-Lopez *et al*, 2014; Post & Clevers, 2019).
490 Our data therefore suggest that under high serum conditions, the Pax7-/ MyHC- transit
491 amplifying cells are replenished via predominantly asymmetric cell divisions of the highly
492 proliferative Pax7+/ MyHC- progenitors, which explains the similar half-life of Pax7+ and
493 Pax7- cell dye dilutions (***Figure 2E,G***). The Pax7-/ MyHC- cells divide slower and likely
494 symmetrically and furthermore continue to be replenished by the asymmetrically dividing
495 progenitors, which explains the exponential expansion of Pax7- cells (***Figure 2F,G***). With

496 terminal differentiation, the Pax7- pool becomes post-mitotic and gradually forms myocytes
497 and myotubes while expressing MyHC (***Figure 2C,G***).
498

499 **K-Ras is needed for progenitor maintenance while H-Ras promotes differentiation**

500 It was previously suggested that the three cancer associated Ras genes, *KRAS*, *NRAS* and *HRAS*
501 all promote muscle differentiation via the PI3K-pathway (Lee *et al*, 2010). However, the
502 individual contributions of the Ras genes on the above established three subpopulations of
503 C2C12 cells is unknown. We therefore utilized siRNA-mediated knockdown to specifically
504 downmodulate endogenous *RAS* isoforms and analyzed the effect on the Pax+/ MyHC-
505 progenitors, Pax7-/ MyHC- transit amplifying cells and Pax7-/ MyHC+ terminally
506 differentiated cells during differentiation.
507 Ras isoform specificity of knockdowns was validated by both immunoblotting (***Figure 3-***
508 ***figure supplement 1***) and quantitative RT-PCR (***Figure 3-figure supplement 2***). This analysis
509 surprisingly revealed that knockdown of *NRAS* significantly increased K-Ras and H-Ras
510 protein expression levels on day 1 (***Figure 3-figure supplement 1F***), which was for K-Ras also
511 reflected on the mRNA-level (***Figure 3-figure supplement 2D***). Hence, this effect is likely not
512 an unspecific siRNA activity, but an endogenous feedback mechanism. In addition, *NRAS*
513 knockdown also downmodulated H-Ras mRNA on day 4 (***Figure 3-figure supplement 2D***).
514 Otherwise, all knockdowns remained isoform specific with an average knockdown efficiency
515 of ≥ 35 % on the protein level during the 5-day differentiation period (***Figure 3-figure***
516 ***supplement 1C,E,G***).
517 Specific knockdown of *KRAS* (i.e., of both K-Ras4A and K-Ras4B proteins) led to a significant
518 reduction of progenitors that is more clearly visible from day 3 onwards (***Figure 3A***).
519 Consequently, a slight but not significant drop in the fraction of transit amplifying cells was
520 noticeable (***Figure 3B***). Importantly, the population of differentiated cells was significantly
521 increased upon *KRAS* knockdown (***Figure 3C***). A similar, albeit attenuated effect notably in
522 the population of differentiated cells was observed with the *NRAS* knockdown (***Figure 3D-F***).
523 It is plausible to assume that the smaller effect is due to the *NRAS* knockdown induced
524 upregulation of K-Ras and H-Ras. A markedly different outcome was observed upon
525 knockdown of *HRAS*, which did not markedly alter the progenitor fraction (***Figure 3G***) but
526 slightly increased the fraction of transit amplifying cells (***Figure 3H***), which then resulted in a
527 significantly decreased fraction of differentiated cells (***Figure 3I***).
528 These population changes are accompanied by a drop in MAPK- and mTORC2-signalling,
529 potentially in an isoform specific manner (***Figure 3 – figure supplement 3***). We observed a

530 decrease of relative Thr202/Tyr204-phosphorylated ERK 1/2 (pERK) levels upon *KRAS* or
531 *HRAS* knockdown, but essentially no change in the case of *NRAS* knockdown (***Figure 3 –***
532 ***figure supplement 3A-D***). Hence, MAPK-signaling is relevant for both progenitor
533 maintenance by K-Ras4A/B (***Figure 3A***) and expansion of differentiated cells by H-Ras
534 (***Figure 3I***). By contrast, downregulation of any *RAS* isoform strongly reduced relative Ser473-
535 phosphorylated Akt1 (pAkt) downstream of Ras and mTORC2 (Kovalski *et al.*, 2019), with
536 the strongest effect for *HRAS* knockdown (***Figure 3 – figure supplement 3E-H***).
537 Taken together, we postulate distinct roles for the three Ras isoforms in regulating C2C12
538 differentiation (***Figure 3J***). K-Ras4A/B proteins are important to maintain the Pax7+
539 progenitor pool and prevent differentiation of the transit amplifying cells (***Figure 3A-C***). N-
540 Ras may have a similar and therefore partially redundant role, which may however be obscured
541 given that its downregulation unexpectedly upregulates K-Ras and to a lesser extent H-Ras
542 (***Figure 3D-F***). This may correspond to a fail-safe mechanism, which makes sense in the
543 context that *NRAS* is the evolutionary more recent Ras gene (Garcia-Espana & Philips, 2023).
544

545 **Oncogenic K-RasG12V blocks differentiation of transit amplifying cells**

546 It is well established that overactive MAPK-activity, such as associated with disease variants
547 of pathway genes, blocks C2C12 cell differentiation (Konieczny *et al*, 1989; Wakioka *et al.*,
548 2001). However, it is unknown, in which subpopulation these defects manifest and whether
549 proliferation is increased, as typically assumed for oncogenic Ras-transformed cells.
550 Both oncogenic mutations as well as overexpression of Ras proteins is found in many cancers.
551 Our flow cytometry-based differentiation assay offers the opportunity to exactly quantitate the
552 expression level-dependent effect of both insults on differentiation, by gating for distinct
553 transient expression levels of mEGFP-tagged wild-type or oncogenic K-Ras4B (hereafter K-
554 Ras). Typically, 2000 – 3000 transfected cells were analyzed per condition, a number that
555 remained constant until day 2 of differentiation, when expression started to drop (***Figure 4-***
556 ***figure supplement 1A,B***). This transient perturbation of differentiation is necessary, as in stable
557 transfectants the homeostasis of the mixed C2C12 cell pool would be permanently disrupted.
558 For both constructs, most cells expressed in an expression window, which we defined as up to
559 10-fold above auto-fluorescence background of untransfected cells (***Figure 4-figure***
560 ***supplement 1C,D***). A high-expression window essentially comprised all cells with expression
561 levels beyond the former threshold.
562 In C2C12 cells expressing wt K-Ras in the low window, the fraction of Pax7+/ MyHC-
563 progenitors remained essentially constant (***Figure 4A***), and at a comparable level to that of

564 untransfected C2C12 cells (***Figure 1D***). As observed for untransfected C2C12 cells (***Figure***
565 ***2A***), a decrease in the pool of transit amplifying Pax7-/ MyHC- cells (***Figure 4B***) was matched
566 by an increase in the number of differentiated Pax7-/ MyHC+ cells (***Figure 4C***). When
567 comparing batch and passage number matched cells it can be inferred that the GFP low window
568 corresponds to more physiological expression conditions. In cells expressing wt K-Ras in the
569 high window, the fraction of progenitor cells appeared unaltered (***Figure 4A***). High wt K-Ras
570 expression then resulted in a decreased fraction of transit amplifying cells as compared to the
571 low-expression window (***Figure 4B***), which was matched by an increased fraction of
572 differentiated cells that again increased over time (***Figure 4C***).
573 The fraction of progenitors appeared likewise unaltered in the GFP low and high windows of
574 cells expressing K-RasG12V (***Figure 4D***). However, the fraction of transformed transit
575 amplifying cells clearly showed a smaller decrease as compared to their wt K-Ras counterparts
576 (***Figure 4E***), irrespective of the expression level. This was matched by a reduced increase of
577 differentiated cells (***Figure 4F***).
578 It is generally assumed that oncogenic Ras mutants increase proliferation, which could impact
579 on the fractions of cells that are analyzed here. We therefore again performed dye-dilution
580 experiments to determine the doubling times in the Pax7+ and Pax7- populations of cells
581 transfected with mEGFP-tagged wt K-Ras and K-RasG12V. Importantly, no significant
582 differences were observed between the cytopainter dye dilution decay half-life values of wt K-
583 Ras and K-RasG12V expressing cells in both the Pax7+ population (***Figure 4G)*** and the Pax7-
584 population (***Figure 4H)***. K-RasG12V therefore does not stimulate proliferation more than the
585 wt counterpart. Instead, K-RasG12V inhibits differentiation of the transit amplifying cells
586 (***Figure 4I***).
587

588 **Oncogenic and RASopathy-associated K-Ras mutants vary in their abilities to block**
589 **differentiation**

590 We next analyzed the impact of various mutant Ras-alleles on C2C12 cell differentiation.
591 Again, we transiently transfected cells with GFP-variant tagged Ras-constructs and examined
592 them by flow-cytometry in the GFP low window. We focused our analysis on day 3 of
593 differentiation, as it is the earliest time point where differentiation measured by the fraction of
594 MyHC+ cells becomes significantly different ($p < 0.0001$) between wt and oncogenic K-Ras
595 in the GFP low window (***Figure 4C, F***). In addition to the most frequent K-Ras mutations
596 (Hobbs *et al*, 2016), we also included N-RasG12V and H-RasG12V and their altered

597 biochemical properties for comparison (***Table S1***) (Hunter *et al*, 2015; Moore *et al.*, 2020;
598 Rabara *et al*, 2019).
599 While the Pax7+/ MyHC- progenitor pool appeared slightly increased by most oncogenic Ras
600 mutants (***Figure 5A***), their ability to block differentiation was most distinct (***Figure 5B***).
601 Interestingly, N-RasG12V and H-RasG12V, like K-RasG12D, left the progenitor fraction
602 unaltered (***Figure 5B***), while significantly blocking differentiation similar to all other
603 oncogenic K-Ras mutants (***Figure 5B***).
604 Aberrant differentiation is also observed in developmental diseases called RASopathies, where
605 Ras-pathway genes are mutated in the germline. Thus, every cell in the body would essentially
606 experience malfunctioning Ras that could broadly impact on development. Consistently, all
607 RASopathies are characterized by multi-organ abnormalities, including of the musculoskeletal
608 system (Stevenson *et al*, 2012). With a few exceptions, *Ras* mutations that are found in
609 RASopathies are different from the ones seen in cancer (Bustelo *et al*, 2018; Castel *et al.*,
610 2020). RASopathy mutants typically display multiple biochemical abnormalities but increase
611 Ras-MAPK signaling less than oncogenic mutants (***Table S2***) (Cirstea *et al.*, 2013; Gremer *et*
612 *al.*, 2011).
613 While the progenitor fractions of K-Ras RASopathy mutant transformed cells were mostly
614 decreased (***Figure 5C***), we saw in general unaltered differentiation or a weaker block of
615 differentiation with RASopathy-derived mutants as compared to oncogenic variants (***Figure***
616 ***5D***). The most obvious exception was K-Ras with the mutation G60R, which inhibited
617 differentiation similar to the weakest oncogenic mutant K-RasG13D. Five other RASopathy
618 mutants also significantly blocked differentiation and three of these were described to be less
619 NF1-GAP sensitive, a defect that is characteristic for all oncogenic mutants (***Table S1***) (Gremer
620 *et al.*, 2011; Schubbert *et al*, 2006). This points to a high significance of the NF1-GAP to
621 facilitate terminal differentiation of transit amplifying cells and implicitly to a disruption of
622 such differentiation steps in general during Ras-driven oncogenesis.
623

624 **K-RasG12C inhibitor profiling reveals their distinct ability to restore differentiation and**
625 **induce toxic cell death**

626 The past few years have seen the arrival of the first direct K-RasG12C inhibitors in the clinic
627 (Punekar *et al*, 2022; Steffen *et al.*, 2023). Classical cell-based assays profile these inhibitors
628 based on their anti-proliferative and cell-killing activity. Here, we have the unique opportunity
629 to quantify to what extent these inhibitors can restore inhibited differentiation that was induced
630 by oncogenic K-Ras alleles.

631 First, we established that the employed DMSO concentrations below 0.1 % that carried over
632 from compound stocks do not impact on differentiation or have toxic effects (***Figure 6-figure***
633 ***supplement 1A,B)***.
634 We then tested the two approved drugs sotorasib (AMG 510) and adagrasib (MRTX849)
635 (Canon *et al.*, 2019; Fell *et al.*, 2020), as well as ARS-1620 the founder of current G12C-
636 inhibitors (Janes *et al.*, 2018), and MRTX1257, a close analogue of MRTX849 (Fell *et al.*,
637 2020).
638 As just described, K-RasG12C decreased the fraction of MyHC+ cells more than K-RasG12V
639 on day 3 (***Figure 6A***). AMG 510 treatment at 3 μM did not have a restorative effect on
640 differentiation of cells expressing wt K-Ras or K-RasG12V, however, it significantly increased
641 the fraction of differentiated cells with K-RasG12C even beyond that of the wt-control (***Figure***
642 ***6A***). This was an interesting observation, as it may indicate a dominant negative action of AMG
643 510-bound K-RasG12C since this phenotype resembles that of the K-RasG12V-S17N with the
644 S17N dominant negative mutation (***Figure 6-figure supplement 1C,D***). This distinct ability of
645 AMG 510 has not been reported previously. As expected, ARS-1620 could fully restore
646 differentiation of K-RasG12C transformed C2C12 cells (***Figure 6B***), while having no effect
647 on the number of intact cells as also observed with AMG 510 (***Figure 6-figure supplement***
648 ***1E,F***).
649 By contrast, neither MRTX1257 nor MRTX849 could fully restore differentiation of K-
650 RasG12C transformed C2C12 cells (***Figure 6C,D***). Instead, we observed a reduction in the
651 MyHC+ fraction in the drug treated K-RasG12V expressing cells (***Figure 6C,D***). This was due
652 to significant general toxicity of these compounds, which led to a significant drop of intact cells
653 even for wt K-Ras expressing cells (***Figure 6-figure supplement 1G,H***).
654
655 We more closely examined this K-RasG12C-inhibitor toxicity using 7-AAD-labelling, which
656 indicates late apoptosis and necrosis in cells (Zembruski *et al*, 2012). This assay confirmed that
657 under otherwise the same conditions the general toxicity increased in the order AMG 510 $\lesssim$
658 ARS-1620 < MRTX1257 $\lesssim$ MRTX 849 in adherent and detached K-RasG12C transformed
659 C2C12 cells (***Figure 6-figure supplement 1I,J***).
660 This analysis demonstrates that both AMG 510 and ARS-1620 are effective and specific K-
661 RasG12C inhibitors that can restore differentiation with no or little non-specific toxicity. On
662 the other hand, both MRTX1257 and MRTX 849 display a broader toxicity, which undermines
663 their differentiation restoring ability.

664

665 **Profiling of clinical and pre-clinical Ras inhibitors for their ability to restore**
666 **differentiation.**

667 In extension of this analysis, we next assessed the oncogene- and allele-specific effect of
668 targeted drugs on differentiation. Altogether we tested eight approved or clinically evaluated
669 Ras-pathway inhibitors at 1 μM (except for trametinib at 0.1 μM and AMG 510 at 3 μM), which
670 target Ras trafficking (tipifarnib and cysmethynil), upstream activation (gefitinib, BI-3406),
671 directly K-Ras (AMG 510, MRTX1133) and the major effector pathways downstream of Ras
672 that are associated with cancer (trametinib, rapamycin).

673 Trafficking inhibitor tipifarnib, which inhibits farnesyltransferase, had a surprisingly broad
674 effect on almost all K-Ras, N-Ras and H-Ras mutants to restore differentiation (***Figure 7A***).
675 By contrast, cysmethynil was essentially inefficacious (***Figure 7A***), in agreement with its
676 clinical performance (Lau *et al*, 2014).

677 The expected H-Ras specificity of tipifarnib treatment becomes more clearly visible, if we
678 consider the net rescue effect of differentiation, i.e. the difference between the MyHC+ fraction
679 with drug treatment and the DMSO-control (***Figure 7B***). The second most sensitive allele was
680 N-RasG12V, interestingly followed by K-RasG12V, while all other oncogenic K-Ras variants
681 were less sensitive. This was surprising, given that K- and N-Ras can undergo its function-
682 restoring alternative prenylation if farnesyltransferase is inhibited (Whyte *et al*, 1997).

683 Upstream inhibitors gefitinib, which blocks EGFR tyrosine kinase activity, only had a modest
684 effect to restore differentiation of some K-Ras alleles (***Figure 7A,B***), which essentially
685 followed the order of the differentiation blocking activity of these K-Ras mutants (***Figure 5B***).
686 The SOS1 inhibitor BI-3406 performed better, leading to a substantial restoration, except for
687 K-RasQ61H, which is known to have an elevated nucleotide exchange activity that allows its
688 activation independent from SOS1 (Gebregiworgis *et al*, 2021; Hofmann *et al*, 2021). By
689 contrast, this compound was more efficient against K-RasG13D with a much-increased
690 nucleotide exchange activity.

691 Next, AMG 510 showed the expected selectivity for K-RasG12C, with a minor effect on other
692 alleles (K-RasG13D, K-RasG12V and N-RasG12V) (***Figure 7A,B***). Allele selectivity, albeit
693 not as clear as with AMG 510, was also seen with the low nanomolar non-covalent K-
694 RasG12D-selective inhibitor MRTX1133 (Wang *et al.*, 2022). Importantly, MRTX1133
695 restored differentiation to the highest levels observed so far for K-RasG12D but did appear to
696 also mildly and non-specifically restore the differentiated fraction in other K-Ras alleles
697 (***Figure 7A,B***). These apparent non-specific effects of the two allele specific inhibitors may

698 arise from non-covalent interactions with the switch II pocket of all K-Ras alleles. For
699 compounds with the MRTX849 scaffold such non-specificity was explicitly demonstrated
700 earlier (Vasta *et al*, 2022).
701 None of the former compounds though exerted an as strong pan-Ras effect as trametinib, which
702 broadly restored differentiation across all alleles and isoforms (***Figure 7A,B***). Only, drugs that
703 have a known allele- or isoform-selectivity (tipifarnib for H-RasG12V, AMG 510 for K-
704 RasG12C and MRTX1133 for K-RasG12D) matched or surpassed the effect of trametinib. This
705 correlated with the clinical success of tipifarnib against H-RasG12V driven tumors and of
706 AMG 510 against K-RasG12C driven tumors (Ho *et al*, 2021; Skoulidis *et al*, 2021). Finally,
707 rapamycin broadly blocked differentiation, consistent with the importance of PI3K/ mTORC1-
708 signaling for myogenesis and terminal differentiation of C2C12 cells (Lee *et al.*, 2010; Xu &
709 Wu, 2000).
710 We therefore, recapitulate closely the *in vivo* effects of targeted pharmacological agents. The
711 broad effect of trametinib moreover highlights the central role of MAPK-activity to block
712 differentiation. This becomes even clearer, when the net restoration of all oncogenic K-Ras
713 alleles by trametinib is analyzed (***Figure 7C***). One recovers a rank-order that anti-correlates
714 with that of rapamycin (***Figure 7D***) and the impact of these alleles on differentiation (***Figure***
715 ***5B***). This suggests that those K-Ras mutants that have a stronger dependence on MAPK-
716 signaling, as expressed by their relative trametinib sensitivity (***Figure 7C***), and lesser
717 dependence on the PI3K/ mTORC1-signaling (***Figure 7D***), more profoundly block
718 differentiation (***Figure 5B***).
719
720

721 **Discussion**

722 The impact of Ras-MAPK-pathway disease mutants on cell transformation and the efficacy of
723 novel Ras drug candidates are typically assessed in a small number of standard assays, such as
724 NIH3T3 transformation and 2D/3D cancer cell proliferation assays, complemented by
725 immunoblotting for markers of Ras-MAPK-pathway activity (Esposito *et al*, 2019). The impact
726 on cell differentiation, though a known hallmark of cancer, has so far been vastly neglected
727 (Chaffer & Weinberg, 2015; Hanahan, 2022).
728 Here we have established the C2C12 cell differentiation model to examine the effect of
729 oncogenic Ras mutants and Ras-pathway drugs on differentiation. Importantly, this model
730 recapitulates typical and fundamental steps of cell differentiation also found *in vivo* (Yin *et al.*,

731 2013). Notably, the NF1 scaffold SPRED1 is induced upon differentiation, concomitant with
732 a drop in MAPK-signaling, which allows to examine this core machinery of Ras-transformation
733 in more detail (Stowe *et al.*, 2012; Wakioka *et al.*, 2001). This implies that our observations
734 have broad implications not only for locally perturbed differentiation in cancer, but also for
735 RASopathies, which are caused by aberrant Ras signaling throughout development. Our
736 approach with a standard commercial cell line is advantageous as compared to the usage of
737 human embryonic stem cells (hESC), which have also been used to identify compounds that
738 maintain stemness or promote differentiation in more laborious, imaging-based high content
739 screens (Barbaric *et al*, 2010; Desbordes *et al*, 2008; Jee *et al*, 2012; Sherman & Pyle, 2013).
740
741 Based on our analysis, we propose a new model on how in the C2C12 cell culture a small
742 number of Pax7+ progenitor myoblasts are maintained, while the majority of cells is primed to
743 differentiate. We suggest that frequent asymmetric divisions maintain the Pax7+/ MyHC-
744 progenitor pool, while generating a transit amplifying Pax7-/ MyHC- pool of cells that
745 exponentially expands within a few symmetric divisions. We furthermore show here that the
746 three cancer associated Ras genes, *KRAS*, *NRAS* and *HRAS* have a distinct, yet partially
747 overlapping involvement in sustaining the proper trajectory from progenitors via here identified
748 transit amplifying cells to differentiated cells. Individual knockdowns generate distinct changes
749 in the three populations that can hardly be explained by the alternative scenario where total Ras
750 levels determine these alterations. Our data suggest a particular relevance of MAPK-signaling
751 for K-Ras4A/B-dependent progenitor maintenance and H-Ras-dependent terminal
752 differentiation. This is consistent with previous reports of MAPK inhibition resulting in
753 increased differentiation (Rommel *et al*, 1999). Our model adds another dimension to currently
754 debated models for the isoform-specific functions of these *Ras* genes, that include differences
755 in plasma membrane organization and effector usage (Mo *et al*, 2018). The generally observed
756 high expression level in particular of K-Ras4B in almost all tissues is consistent with its major
757 function to sustain progenitors and being the evolutionary most ancient Ras isoform (Garcia-
758 Espana & Philips, 2023; Hood *et al.*, 2023).
759
760 It is well established that oncogenic Ras, constitutively active Raf or MEK1 inhibit myoblast
761 differentiation (Dorman & Johnson, 1999; Olson *et al*, 1987; Weyman & Wolfman, 1998).
762 However, we observed two distinct types of perturbed differentiation by Ras-pathway
763 hyperactivation. The first is associated with overexpression of wt K-Ras that led to a more
764 pronounced drop in the transit amplifying population matched by a significantly increased

765 differentiation. By contrast, all NF1-GAP insensitive oncogenic Ras variants blocks terminal
766 differentiation as compared to wt K-Ras. Moreover, those mutants that show a stronger
767 sensitivity to trametinib and a lower sensitivity to rapamycin, are more potent to block
768 differentiation. This order does not exactly fit with the mutation frequency of the oncogenic K-
769 Ras alleles, but it could reflect their severity as expressed by the overall survival associated
770 with the mutants. And exception is K-RasG13D, which is a biochemical outlier with a high
771 nucleotide exchange rate, high intrinsic GTPase activity and NF1-GAP sensitivity (Hunter *et*
772 *al.*, 2015; Rabara *et al.*, 2019).
773 As already inferred from their biochemical characterization, RASopathy associated K-Ras
774 mutants are not or less able to block differentiation, consistent with these alterations being
775 compatible with organismal development. Instead, it appears that many of them are defective
776 in sustaining the C2C12 cell progenitor fraction. Intriguingly, the most potent RASopathy
777 mutant K-RasG60R, which inhibits differentiation as much as the weaker oncogenic K-Ras
778 allele K-RasG12V, also displays a more prominent NF1-GAP resistance. The milder effects of
779 RASopathy K-Ras mutants G60R and P34R can be explained by their decreased effector
780 engagement, which also exists in a milder manifestation in the V14I mutant. We postulate that
781 both K5-mutants also impact on NF1-GAP activity in the cell, given their ability to
782 significantly block differentiation.
783 We speculate that for all of these NF1-GAP resistant mutants, differentiation of transit
784 amplifying cells is blocked, as shown for K-RasG12V. This is consistent with the fact that with
785 the induction of differentiation, the potentially K-Ras-selective tumor suppressor complex of
786 SPRED1 with the GAP NF1 can become active only after SPRED1-induction (Siljamaki &
787 Abankwa, 2016; Stowe *et al.*, 2012; Wakioka *et al.*, 2001). Thus, MAPK-signaling would be
788 sustained in transit amplifying cells, which prevents differentiation. This specifies that the
789 oncogenic insult of hotspot-mutated Ras occurs at a defined point of the differentiation
790 trajectory, an important fact that has not been recognized before. Moreover, this model implies
791 molecular mechanistic and developmental commonalities between cancer and RASopathies,
792 which have been long elusive (Castel *et al.*, 2020).
793
794 In direct correlation with our muscle cell line observations, RASopathy patients display muscle
795 weakness in particular in Costello syndrome (CS) (Stevenson *et al.*, 2012; Stevenson & Yang,
796 2011). In the heterozygous G12V CS mouse model a decreased muscle mass and strength was
797 found, due to inhibited embryonic myogenesis and myofiber formation (Tidyman *et al*, 2022).
798 This was due to an inhibited differentiation in the embryonic muscles, with a 23 % increase in

799 Pax7 expressing cells and a decrease in MyoD and myogenin expressing cells to 60-70 % of
800 the wt. A less severe skeletal myopathy is observed in the RASopathy cardiofaciocutaneous
801 syndrome mouse model with a BRAF-L597V mutation (Maeda *et al*, 2021). Given the distinct
802 penetrance of muscle phenotypes in RASopathies, one may assume this could be due to distinct
803 mutant allele strengths, as suggested by our data. Alternatively, in muscle cells only certain
804 alleles could become significant, while others would be tissue specifically contained, which is
805 probably a less likely scenario. Importantly, these data corroborate the idea that the muscle
806 phenotype in RASopathies is due to perturbed differentiation of stem/ progenitor cells, as has
807 been observed in other muscle diseases notably in Duchenne muscular dystrophy, where
808 asymmetric cell divisions of satellite cells are likewise not proceeding correctly (Feige *et al*,
809 2018).
810 Soft tissue rhabdomyosarcoma (RMS) of the muscle are frequently observed in RASopathies,
811 such as Neurofibromatosis type 1, Noonan syndrome and CS (Skapek *et al*, 2019). RMS is the
812 most common childhood soft-tissue sarcoma with only 30 % survival in the metastatic disease.
813 These tumors emerge from muscle progenitors/ myoblasts that failed to differentiate, albeit the
814 exact cell of origin is still not well characterized (Skapek *et al.*, 2019). Strikingly, this is exactly
815 the phenotype we have observed in our data.
816 Two RMS subtypes are distinguished, the alveolar type in adolescents and the embryonal type
817 in younger patients, which is associated with good prognosis, despite higher mutational burden
818 (Shern *et al*, 2014). The former largely overlaps with the Pax-fusion positive molecular
819 subtype, with neomorphic gain-of-function fusion proteins of Pax3 or Pax7 with FOXO1. In
820 the Pax-fusion negative (embryonal) subtype of RMS, the Ras-pathway is activated by
821 mutations in the pathway, while in the Pax-fusion positive subtype the upregulation of Ras
822 pathway genes is found (Shern *et al.*, 2014; Skapek *et al.*, 2019). Interestingly, it is one of the
823 few cancer types where the three Ras isoforms are mutated at about equal frequency.
824 Oncogenic Ras prevents differentiation in rhabdomyosarcoma (Yohe *et al*, 2018).
825
826 Finally, we profiled the effect of drugs on differentiation in a rapid and unique manner. Our
827 assessment of four K-Ras-G12C inhibitors importantly demonstrates that inhibition of the
828 oncogenic K-Ras also rescues differentiation. Yet, unexpected idiosyncrasies of these
829 compounds were observed. Interestingly, the increase in differentiation that we observed with
830 K-RasG12C bound AMG 510, may suggest a molecular complex that becomes dominant
831 negative, similar to what is seen with S17N-mutation. It is not likely that target-independent,
832 off-target effects are responsible for this observation, as there is no effect with K-RasG12V

833 expressing cells. By contrast, adagrasib (MRTX849) and more so MRTX1257 were less
834 proficient in restoring differentiation, while inducing significantly more non-specific cell
835 death. This is typically not desired, and in this particular case it may be attributed to the
836 inhibition of wt K-Ras (Vasta *et al.*, 2022). Their inhibition of other mutant *KRAS* alleles is
837 probably beneficial in the clinical setting, where any antiproliferative activity could be helpful
838 and the activity against other *KRAS* alleles prevents their success if they evolved as a resistance
839 mechanism (Liu *et al*, 2022).
840 Consistent with observations in the more complex hESC model and zebra fish larvae (Chen *et*
841 *al*, 2011; Pal *et al*, 2012), we also noted the significant, dose-dependent effect of DMSO at
842 concentrations above 0.2 % on C2C12 cell differentiation and viability. Hence, our assay may
843 be suitable to identify and explain differentiation perturbing, toxic effects of organic solvents
844 or other substances that may correlate with their teratogenic potential.
845 We furthermore illustrate the enormous potential for Ras-pathway drug profiling on multiple
846 Ras-disease mutants in our 8 × 8 matrix, which revealed a remarkable correlation of the ability
847 of drugs to restore differentiation with their clinical efficacy in Ras disease treatment.
848 Trametinib was very efficacious to restore differentiation of K-Ras mutants that profoundly
849 blocked differentiation. Interestingly, the same order of sensitivity was found for tipifarnib,
850 which may indicate that both drugs, tipifarnib and trametinib could work synergistically to
851 block differentiation. The broad capacity to restore differentiation by MEK-inhibition is
852 paralleled by results obtained with myocyte cultures derived from the CS mouse model.
853 Differentiation of those cells could be restored by the MEK inhibitor PD0325901, while the
854 differentiation of the wt control was further increased. Importantly, this was mirrored by
855 muscle-mass and -diameter increases *in vivo* to control levels (Tidyman *et al.*, 2022). Thus,
856 relative muscle strength development in RASopathy patients may also serve as a biomarker for
857 treatment efficacy. We found that rapamycin was one of the few compounds, which prevented
858 C2C12 cell differentiation. Others have previously shown that it inhibits differentiation that is
859 promoted by the PI3K/ mTORC1- pathway (Hatfield *et al*, 2015). While the PI3K/ Akt/
860 mTORC1/ S6K1-axis is involved in hypertrophic muscle growth (Mounier *et al*, 2011; Yoon,
861 2017), the PI3K inhibitor GDC0941 led to muscle cell death in a CS mouse model and was
862 deleterious *in vivo* (Tidyman *et al.*, 2022). However, in the aging muscle, hyperactive
863 mTORC1 appears to induce muscle damage and loss, hence low dose treatment with rapamycin
864 analogue everolimus (RAD001) salvages this situation *in vivo* (Joseph *et al*, 2019). In the end,
865 this compound analysis allowed us to estimate the utilization of the MAPK- and PI3K-pathway
866 suggesting that oncogenic K-Ras alleles show a distinct dependence on these pathways.

867 Interestingly, those mutants with a higher MAPK (trametinib)- and lower PI3K/ mTORC1
868 (rapamycin) -dependence were more potent to block differentiation.
869
870 Future developments of such drug-profiling derived models may enable us to predict
871 efficacious drug combination that do not only restore differentiation but in parallel also work
872 in cancer therapy. The fact that we observe striking correlations of our differentiation data with
873 overall Ras mutation strength and drug-responses observed in the clinic, suggests that we are
874 looking here at a highly conserved function of Ras that is deeply engrained into the functioning
875 of nearly every metazoan cell system. In order to devise therapies that can fully salvage the
876 aberrant differentiation induced by Ras-pathway hyperactivation, we need to understand its
877 impact on both cell proliferation and differentiation. The involvement of Ras beyond the G1-
878 phase, where the Ras-MAPK pathway is known to drive S-phase entry such as by stimulating
879 cyclin D expression, is largely unknown. However, cell fate decisions are taken during M-
880 phase, as stem/ progenitor cells symmetrically or asymmetrically divide. We therefore
881 postulate a distinct role of Ras-pathway activity during this fundamental step, which cannot
882 merely be explained by different strengths of the pathway output, but the underlying cell and
883 developmental biology.
884

885 **Resource availability**

886 ***Lead contact***

887 Further information and requests for resources and reagents should be directed to and will be
888 fulfilled by the lead contact, Daniel Kwaku Abankwa (daniel.abankwa@uni.lu).

889 ***Materials availability***

890 This study did not generate new unique reagents.

891 ***Data and code availability***

892 No standardized datasets were produced within this study.
893

894 **Acknowledgements**

895 This work was supported by a grant from the Luxembourg National Research Fund (FNR)
896 grant C19/BM/13673303-PolaRAS2 to D.K.A.
897

898 **Author contributions**

899 R.C. and D.K.A participated in the initial conceptualization. R.C. and B.P. designed and carried
900 out flow cytometry experiments and data analysis. C.L collected and evaluated immunoblot
901 and qPCR data for RAS isoform knockdown. F.K acquired immunoblot data for differentiation
902 marker expression and performed 7AAD-cell toxicity assay. N.B.F generated expression
903 constructs via gateway cloning. R.C., B.P. and D.K.A wrote the first draft of the manuscript.
904 D.K.A. edited the manuscript and supervised the entire study.

905

906 **Declaration of interests**

907 The authors declare no competing interests.

908

909

910

911

912 **Figure legends**

913 **Figure 1. Improved characterization of C2C12 cell differentiation by flow cytometry.** (**A**)
914 Differentiation of skeletal muscle *in vivo* (top) and of C2C12 cells (bottom) are similar based
915 on marker expression.
916 (**B**) C2C12 cells were differentiated by switching to low serum medium for indicated times.
917 Brightfield images were obtained at 10 × magnification. Scale bars, 200 µm.
918 (**C-H**) Representative immunoblots and quantification of Pax7 (C), myogenin (E) and MyHC
919 (G) expression in C2C12 cells; N = 3, passage number 6. Representative flow cytometry
920 histograms of marker+ cells at indicated times after serum switch (left). Quantification of
921 marker+ fraction and geometric means of intensities (right). Analyzed markers were Pax7 (D),
922 myogenin (F) and MyHC (H); N = 3, passage number 6. Statistical significance was calculated
923 using the Friedman's test and Dunn's post hoc test in comparison to day 0. The switch to low
924 serum medium for differentiation is here and subsequently indicated with a vertical dashed
925 line.
926
927
928 **Figure 2. A major pool of Pax7-/ MyHC- transit amplifying cells gives rise to Pax7-/**
929 **MyHC+ differentiated cells.** (**A**) Flow cytometric analysis of C2C12 cell subpopulations after
930 indicated times of differentiation; N ≥ 2, passage number 8-9.
931 (**B,C**) Quantification of mitotically active (pH3+) Pax7+ (B) and Pax7- (C) subpopulations; N
932 = 4, passage number 7-8.
933 (**D**) Representative histograms of cytopainter dye dilution experiments from C2C12 cells
934 proliferating in high serum medium for indicated times. Inset schematic illustrates dye dilution
935 upon division.
936 (**E**) Quantification of dye dilution experiments as in (D). Geometric means of fluorescence
937 intensities of cytopainter deep red-labelled Pax7+ and Pax7- cells; N = 3, passage number 7-8.
938 Half-life ($t_{1/2}$) of each fluorescence decay was calculated as described in methods.
939 (**F**) Analysis of cell concentrations of Pax7+ and Pax7- populations proliferating in high serum;
940 N = 3, passage number 7-8.
941 (**G**) Revised population model for C2C12 cells. Our data suggest that Pax7+/ MyHC-
942 progenitors divide to some extent symmetrically (boxed), but mostly asymmetrically, to self-
943 renew and expand the number of slowly proliferating Pax7-/ MyHC- transit amplifying cells.
944 This major pool of cells can be triggered to differentiate into Pax7-/ MyHC+ cells in low serum.

945
946
947 **Figure 3. K-Ras4A/4B block whereas H-Ras promotes C2C12 differentiation.** (**A-I**) Flow
948 cytometric quantification of double-labelled C2C12 cells at indicated times of differentiation.
949 At day 0 cells were treated with si*KRAS* to knock down both isoforms K-Ras4A/4B or control
950 siRNA (CTRL) (A-C). Analogous treatments were done using si*NRAS* (D-F) or si*HRAS* (G-I).
951 Then the fractions of Pax7+/ MyHC- progenitors (A,D,G), Pax7-/ MyHC- transit amplifying
952 cells (B,E,H) and Pax7-/ MyHC+ differentiated cells (C,F,I) were determined by flow
953 cytometric analysis. Ideograms of cells at the top indicate the analyzed cell population in the
954 column of panels; N ≥ 4, passage number 6-7.
955 (**J**) Update of our population model for C2C12 cell differentiation with inferred participation
956 of Ras isoforms in cell divisions.
957
958
959 **Figure 4. Oncogenic K-Ras4B blocks differentiation of transit amplifying cells.** (**A-C**)
960 Flow cytometric analysis of temporal evolution of Pax7+/ MyHC- progenitors (A), Pax7-/
961 MyHC- transit amplifying cells (B) and Pax7-/ MyHC+ differentiated cells (C) after
962 transfection of C2C12 cells with mEGFP tagged wt K-Ras on day 0. Cells in the GFP low and
963 GFP high expression windows were analyzed; N = 3, passage number 6.
964 (**D-F**) Flow cytometric analysis of temporal evolution of Pax7+/ MyHC- progenitors (D),
965 Pax7-/ MyHC- transit amplifying cells (E) and Pax7-/ MyHC+ differentiated cells (F) after
966 transfection of C2C12 cells with mEGFP tagged oncogenic K-RasG12V on day 0. Cells in the
967 GFP low and GFP high expression windows were analyzed; N = 3, passage number 6.
968 (**G,H**) Geometric means of fluorescence intensities of cytopainter orange-labelled Pax7+ (G)
969 and Pax7- (H) of mEGFP-wt K-Ras or mEGFP-K-RasG12V expressing C2C12 cells; N = 3,
970 passage number 6. Half-life ($t_{1/2}$) of each fluorescence decay was calculated as described in
971 methods.
972 (**I**) Population model for C2C12 cells transformed with oncogenic K-RasG12V, which blocks
973 differentiation at the level of Pax7-/ MyHC- transit amplifying cells.
974
975
976 **Figure 5. All oncogenic Ras mutants block differentiation, while RASopathy associated**
977 **K-Ras mutants affect differentiation more broadly.** (**A,B**) EGFP-variant tagged oncogenic
978 Ras constructs were transfected into C2C12 cells on day 0 and subsequently on day 3 of

979 differentiation Pax7+ cell fractions (A) and MyHC+ cell fractions (B) were analyzed by flow
980 cytometry; N = 3, passage number 7.
981 (**C,D**) EYFP-tagged K-Ras RASopathy mutants were transfected into C2C12 cells on day 0
982 and subsequently on day 3 of differentiation Pax7+ cell fractions (A) and MyHC+ cell fractions
983 (B) were analyzed by flow cytometry; N ≥ 2, passage number 9.
984 In all plots, at least 3000 cells in the GFP low expression windows were analyzed.
985
986
987 **Figure 6. K-RasG12C inhibitor profiling reveals their distinct ability to restore**
988 **differentiation.** (**A-D**) Analysis of MyHC+ C2C12 cell fractions expressing GFP-variant
989 tagged wt K-Ras, K-RasG12V and K-RasG12C on day 3 of differentiation. From day 1
990 onwards 3 μM of AMG 510 (A), ARS-1620 (B), MRTX1257 (C) or MRTX849 (D) or vehicle
991 (DMSO 0.1 % v/v) were added to cells; N = 4.
992 In all plots, only cells from passage 9 in the GFP low expression windows were analyzed.
993
994
995 **Figure 7. Profiling of clinically tested Ras inhibitors for their ability to restore**
996 **differentiation.** (**A**) Heatmap showing % MyHC+ C2C12 cells, i.e. the absolute rescue effect,
997 on day 3 of differentiation for each indicated condition. EGFP-variant tagged Ras-constructs
998 were transfected on day 0; N = 3, passage number 7. The scale to the right shows the wt K-Ras
999 differentiation level as a reference.
1000 (**B**) Net rescue effect of drugs. Data from (A) were used by subtracting values from vehicle
1001 control (DMSO 0.2 % v/v) treated samples in the top row from those treated with drugs. The
1002 scale to the right shows the DMSO-control level as a reference.
1003 (**C**) Extract of data from (B). MAPK-pathway dependence of K-Ras variants judged by the
1004 trametinib induced net rescue.
1005 (**D**) Extract of data from (B). PI3K/ mTORC1-pathway dependence of K-Ras variants judged
1006 by the rapamycin induced net rescue.
1007 In all plots, only cells in the GFP low expression windows were analyzed.
1008

1009

1010

1011 **References**

1012 (2022) The KRAS(G12D) inhibitor MRTX1133 elucidates KRAS-mediated oncogenesis. *Nat*
1013 *Med* 28: 2017-2018

1014 Abankwa D, Gorfe AA, Inder K, Hancock JF (2010) Ras membrane orientation and
1015 nanodomain localization generate isoform diversity. *Proc Natl Acad Sci U S A* 107: 1130-1135

1016 Ahmadian MR, Stege P, Scheffzek K, Wittinghofer A (1997) Confirmation of the arginine-
1017 finger hypothesis for the GAP-stimulated GTP-hydrolysis reaction of Ras. *Nat Struct Biol* 4: 686-689

1018 Altshuler A, Verbuk M, Bhattacharya S, Abramovich I, Haklai R, Hanna JH, Kloog Y, Gottlieb
1019 E, Shalom-Feuerstein R (2018) RAS Regulates the Transition from Naive to Primed Pluripotent Stem
1020 Cells. *Stem Cell Reports* 10: 1088-1101

1021 Ansieau S (2013) EMT in breast cancer stem cell generation. *Cancer Letters* 338: 63-68

1022 Barbaric I, Gokhale PJ, Jones M, Glen A, Baker D, Andrews PW (2010) Novel regulators of
1023 stem cell fates identified by a multivariate phenotype screen of small compounds on human embryonic
1024 stem cell colonies. *Stem Cell Res* 5: 104-119

1025 Barretina J, Caponigro G, Stransky N, Venkatesan K, Margolin AA, Kim S, Wilson CJ, Lehar
1026 J, Kryukov GV, Sonkin D *et al* (2012) The Cancer Cell Line Encyclopedia enables predictive modelling
1027 of anticancer drug sensitivity. *Nature* 483: 603-607

1028 Batlle E, Clevers H (2017) Cancer stem cells revisited. *Nat Med* 23: 1124-1134

1029 Bennett AM, Tonks NK (1997) Regulation of distinct stages of skeletal muscle differentiation
1030 by mitogen-activated protein kinases. *Science* 278: 1288-1291

1031 Brems H, Pasmant E, Van Minkelen R, Wimmer K, Upadhyaya M, Legius E, Messiaen L
1032 (2012) Review and update of SPRED1 mutations causing Legius syndrome. *Hum Mutat* 33: 1538-1546

1033 Brown DM, Parr T, Brameld JM (2012) Myosin heavy chain mRNA isoforms are expressed in
1034 two distinct cohorts during C2C12 myogenesis. *J Muscle Res Cell Motil* 32: 383-390

1035 Bustelo XR, Crespo P, Fernandez-Pisonero I, Rodriguez-Fdez S (2018) RAS GTPase-
1036 dependent pathways in developmental diseases: old guys, new lads, and current challenges. *Curr Opin*
1037 *Cell Biol* 55: 42-51

1038 Canon J, Rex K, Saiki AY, Mohr C, Cooke K, Bagal D, Gaida K, Holt T, Knutson CG, Koppada
1039 N *et al* (2019) The clinical KRAS(G12C) inhibitor AMG 510 drives anti-tumour immunity. *Nature*
1040 575: 217-223

1041 Castel P, Rauen KA, McCormick F (2020) The duality of human oncoproteins: drivers of
1042 cancer and congenital disorders. *Nat Rev Cancer* 379: 1-15

1043 Chaffer CL, Weinberg RA (2015) How does multistep tumorigenesis really proceed? *Cancer*
1044 *Discov* 5: 22-24

1045 Chen TH, Wang YH, Wu YH (2011) Developmental exposures to ethanol or dimethylsulfoxide
1046 at low concentrations alter locomotor activity in larval zebrafish: implications for behavioral toxicity
1047 bioassays. *Aquat Toxicol* 102: 162-166

1048 Chia W, Somers WG, Wang H (2008) Drosophila neuroblast asymmetric divisions: cell cycle
1049 regulators, asymmetric protein localization, and tumorigenesis. *J Cell Biol* 180: 267-272

1050 Chippalkatti R, Abankwa D (2021) Promotion of cancer cell stemness by Ras. *Biochem Soc*
1051 *Trans* 49: 467-476

1052 Cirstea IC, Gremer L, Dvorsky R, Zhang SC, Piekorz RP, Zenker M, Ahmadian MR (2013)
1053 Diverging gain-of-function mechanisms of two novel KRAS mutations associated with Noonan and
1054 cardio-facio-cutaneous syndromes. *Hum Mol Genet* 22: 262-270

1055 Crespo P, Leon J (2000) Ras proteins in the control of the cell cycle and cell differentiation.
1056 *Cell Mol Life Sci* 57: 1613-1636

1057 de Alvaro C, Martinez N, Rojas JM, Lorenzo M (2005) Sprouty-2 overexpression in C2C12
1058 cells confers myogenic differentiation properties in the presence of FGF2. *Mol Biol Cell* 16: 4454-4461
1059 Desbordes SC, Placantonakis DG, Ciro A, Socci ND, Lee G, Djaballah H, Studer L (2008)
1060 High-throughput screening assay for the identification of compounds regulating self-renewal and
1061 differentiation in human embryonic stem cells. *Cell Stem Cell* 2: 602-612
1062 Dontu G, Abdallah WM, Foley JM, Jackson KW, Clarke MF, Kawamura MJ, Wicha MS (2003)
1063 In vitro propagation and transcriptional profiling of human mammary stem/progenitor cells. *Genes Dev*
1064 17: 1253-1270
1065 Dorman CM, Johnson SE (1999) Activated Raf inhibits avian myogenesis through a MAPK-
1066 dependent mechanism. *Oncogene* 18: 5167-5176
1067 Duggan MC, Regan-Fendt K, Olaverria Salavaggione GN, Howard JH, Stiff AR, Sabella J,
1068 Latchana N, Markowitz J, Gru A, Tridandapani S *et al* (2019) Neuroblastoma RAS viral oncogene
1069 homolog mRNA is differentially spliced to give five distinct isoforms: implications for melanoma
1070 therapy. *Melanoma Res* 29: 491-500
1071 Esposito D, Stephen AG, Turbyville TJ, Holderfield M (2019) New weapons to penetrate the
1072 armor: Novel reagents and assays developed at the NCI RAS Initiative to enable discovery of RAS
1073 therapeutics. *Semin Cancer Biol* 54: 174-182
1074 Feige P, Brun CE, Ritso M, Rudnicki MA (2018) Orienting Muscle Stem Cells for
1075 Regeneration in Homeostasis, Aging, and Disease. *Cell Stem Cell* 23: 653-664
1076 Fell JB, Fischer JP, Baer BR, Blake JF, Bouhana K, Briere DM, Brown KD, Burgess LE, Burns
1077 AC, Burkard MR *et al* (2020) Identification of the Clinical Development Candidate MRTX849, a
1078 Covalent KRAS(G12C) Inhibitor for the Treatment of Cancer. *J Med Chem* 63: 6679-6693
1079 Garcia-Espana A, Philips MR (2023) Origin and Evolution of RAS Membrane Targeting.
1080 *Oncogene* 42: 1741-1750
1081 Gebregiworgis T, Kano Y, St-Germain J, Radulovich N, Udaskin ML, Mentes A, Huang R,
1082 Poon BPK, He W, Valencia-Sama I *et al* (2021) The Q61H mutation decouples KRAS from upstream
1083 regulation and renders cancer cells resistant to SHP2 inhibitors. *Nat Commun* 12: 6274
1084 Golebiewska A, Brons NH, Bjerkvig R, Niclou SP (2011) Critical appraisal of the side
1085 population assay in stem cell and cancer stem cell research. *Cell Stem Cell* 8: 136-147
1086 Gomez-Lopez S, Lerner RG, Petritsch C (2014) Asymmetric cell division of stem and
1087 progenitor cells during homeostasis and cancer. *Cell Mol Life Sci* 71: 575-597
1088 Goto H, Tomono Y, Ajiro K, Kosako H, Fujita M, Sakurai M, Okawa K, Iwamatsu A, Okigaki
1089 T, Takahashi T, Inagaki M (1999) Identification of a novel phosphorylation site on histone H3 coupled
1090 with mitotic chromosome condensation. *J Biol Chem* 274: 25543-25549
1091 Gremer L, Merbitz-Zahradnik T, Dvorsky R, Cirstea IC, Kratz CP, Zenker M, Wittinghofer A,
1092 Ahmadian MR (2011) Germline KRAS mutations cause aberrant biochemical and physical properties
1093 leading to developmental disorders. *Hum Mutat* 32: 33-43
1094 Gross AM, Frone M, Gripp KW, Gelb BD, Schoyer L, Schill L, Stronach B, Biesecker LG,
1095 Esposito D, Hernandez ER *et al* (2020) Advancing RAS/RASopathy therapies: An NCI-sponsored
1096 intramural and extramural collaboration for the study of RASopathies. *Am J Med Genet A* 182: 866-
1097 876
1098 Gupta PB, Onder TT, Jiang G, Tao K, Kuperwasser C, Weinberg RA, Lander ES (2009)
1099 Identification of selective inhibitors of cancer stem cells by high-throughput screening. 138: 645-659
1100 Haghighi F, Dahlmann J, Nakhaei-Rad S, Lang A, Kutschka I, Zenker M, Kensah G, Piekorz
1101 RP, Ahmadian MR (2018) bFGF-mediated pluripotency maintenance in human induced pluripotent
1102 stem cells is associated with NRAS-MAPK signaling. *Cell Commun Signal* 16: 96
1103 Hanahan D (2022) Hallmarks of Cancer: New Dimensions. *Cancer Discov* 12: 31-46
1104 Hatfield I, Harvey I, Yates ER, Redd JR, Reiter LT, Bridges D (2015) The role of TORC1 in
1105 muscle development in Drosophila. *Sci Rep* 5: 9676

1106 Ho AL, Brana I, Haddad R, Bauman J, Bible K, Oosting S, Wong DJ, Ahn MJ, Boni V, Even
1107 C *et al* (2021) Tipifarnib in Head and Neck Squamous Cell Carcinoma With HRAS Mutations. *J Clin*
1108 *Oncol* 39: 1856-1864

1109 Hobbs GA, Der CJ, Rossman KL (2016) RAS isoforms and mutations in cancer at a glance. *J*
1110 *Cell Sci* 129: 1287-1292

1111 Hofmann MH, Gmachl M, Ramharter J, Savarese F, Gerlach D, Marszalek JR, Sanderson MP,
1112 Kessler D, Trapani F, Arnhof H *et al* (2021) BI-3406, a Potent and Selective SOS1-KRAS Interaction
1113 Inhibitor, Is Effective in KRAS-Driven Cancers through Combined MEK Inhibition. *Cancer Discov*
1114 11: 142-157

1115 Hood FE, Sahraoui YM, Jenkins RE, Prior IA (2023) Ras protein abundance correlates with
1116 Ras isoform mutation patterns in cancer. *Oncogene* 42: 1224-1232

1117 Hunter JC, Manandhar A, Carrasco MA, Gurbani D, Gondi S, Westover KD (2015)
1118 Biochemical and Structural Analysis of Common Cancer-Associated KRAS Mutations. *Mol Cancer*
1119 *Res* 13: 1325-1335

1120 Janes MR, Zhang J, Li LS, Hansen R, Peters U, Guo X, Chen Y, Babbar A, Firdaus SJ, Darjania
1121 L *et al* (2018) Targeting KRAS Mutant Cancers with a Covalent G12C-Specific Inhibitor. *Cell* 172:
1122 578-589 e517

1123 Jee J, Jeon H, Hwang D, Sommer P, Park Z, Cechetto J, Dorval T (2012) High content screening
1124 for compounds that induce early stages of human embryonic stem cell differentiation. *Comb Chem High*
1125 *Throughput Screen* 15: 656-665

1126 Jindal GA, Goyal Y, Burdine RD, Rauen KA, Shvartsman SY (2015) RASopathies: unraveling
1127 mechanisms with animal models. *Dis Model Mech* 8: 769-782

1128 Joseph GA, Wang SX, Jacobs CE, Zhou W, Kimble GC, Tse HW, Eash JK, Shavlakadze T,
1129 Glass DJ (2019) Partial Inhibition of mTORC1 in Aged Rats Counteracts the Decline in Muscle Mass
1130 and Reverses Molecular Signaling Associated with Sarcopenia. *Mol Cell Biol* 39

1131 Konieczny SF, Drobes BL, Menke SL, Taparowsky EJ (1989) Inhibition of myogenic
1132 differentiation by the H-ras oncogene is associated with the down regulation of the MyoD1 gene.
1133 *Oncogene* 4: 473-481

1134 Kovalski JR, Bhaduri A, Zehnder AM, Neela PH, Che Y, Wozniak GG, Khavari PA (2019)
1135 The Functional Proximal Proteome of Oncogenic Ras Includes mTORC2. *Mol Cell* 73: 830-844 e812

1136 Laplante M, Sabatini DM (2013) Regulation of mTORC1 and its impact on gene expression at
1137 a glance. *J Cell Sci* 126: 1713-1719

1138 Lassar AB, Thayer MJ, Overell RW, Weintraub H (1989) Transformation by activated ras or
1139 fos prevents myogenesis by inhibiting expression of MyoD1. *Cell* 58: 659-667

1140 Lau HY, Ramanujulu PM, Guo D, Yang T, Wirawan M, Casey PJ, Go ML, Wang M (2014)
1141 An improved isoprenylcysteine carboxylmethyltransferase inhibitor induces cancer cell death and
1142 attenuates tumor growth in vivo. *Cancer Biol Ther* 15: 1280-1291

1143 Lee J, Choi KJ, Lim MJ, Hong F, Choi TG, Tak E, Lee S, Kim YJ, Chang SG, Cho JM *et al*
1144 (2010) Proto-oncogenic H-Ras, K-Ras, and N-Ras are involved in muscle differentiation via
1145 phosphatidylinositol 3-kinase. *Cell Res* 20: 919-934

1146 Li C, Vides A, Kim D, Xue JY, Zhao Y, Lito P (2021) The G protein signaling regulator RGS3
1147 enhances the GTPase activity of KRAS. *Science* 374: 197-201

1148 Li W, Ma H, Zhang J, Zhu L, Wang C, Yang Y (2017) Unraveling the roles of CD44/CD24
1149 and ALDH1 as cancer stem cell markers in tumorigenesis and metastasis. *Sci Rep* 7: 13856

1150 Liu J, Kang R, Tang D (2022) The KRAS-G12C inhibitor: activity and resistance. *Cancer Gene*
1151 *Ther* 29: 875-878

1152 Livak KJ, Schmittgen TD (2001) Analysis of relative gene expression data using real-time
1153 quantitative PCR and the 2(-Delta Delta C(T)) Method. *Methods* 25: 402-408

1154 Maeda Y, Tidyman WE, Ander BP, Pritchard CA, Rauen KA (2021) Ras/MAPK dysregulation
1155 in development causes a skeletal myopathy in an activating Braf(L597V) mouse model for cardio-facio-
1156 cutaneous syndrome. *Dev Dyn* 250: 1074-1095

1157 Mathews LA, Keller JM, Goodwin BL, Guha R, Shinn P, Mull R, Thomas CJ, de Kluyver RL,
1158 Sayers TJ, Ferrer M (2012) A 1536-well quantitative high-throughput screen to identify compounds
1159 targeting cancer stem cells. *J Biomol Screen* 17: 1231-1242
1160 McDonald ER, 3rd, de Weck A, Schlabach MR, Billy E, Mavrakis KJ, Hoffman GR, Belur D,
1161 Castelletti D, Frias E, Gampa K *et al* (2017) Project DRIVE: A Compendium of Cancer Dependencies
1162 and Synthetic Lethal Relationships Uncovered by Large-Scale, Deep RNAi Screening. *Cell* 170: 577-
1163 592 e510
1164 Mo SP, Coulson JM, Prior IA (2018) RAS variant signalling. *Biochem Soc Trans* 46: 1325-
1165 1332
1166 Moore AR, Rosenberg SC, McCormick F, Malek S (2020) RAS-targeted therapies: is the
1167 undruggable drugged? *Nat Rev Drug Discov* 19: 533-552
1168 Morrison SJ, Kimble J (2006) Asymmetric and symmetric stem-cell divisions in development
1169 and cancer. *Nature* 441: 1068-1074
1170 Mounier R, Lantier L, Leclerc J, Sotiropoulos A, Foretz M, Viollet B (2011) Antagonistic
1171 control of muscle cell size by AMPK and mTORC1. *Cell Cycle* 10: 2640-2646
1172 Najumudeen AK, Jaiswal A, Lectez B, Oetken-Lindholm C, Guzman C, Siljamaki E, Posada
1173 IM, Lacey E, Aittokallio T, Abankwa D (2016) Cancer stem cell drugs target K-ras signaling in a
1174 stemness context. *Oncogene* 35: 5248-5262
1175 Nassar D, Blanpain C (2016) Cancer Stem Cells: Basic Concepts and Therapeutic Implications.
1176 *Annu Rev Pathol* 11: 47-76
1177 Norris SR, Nunez MF, Verhey KJ (2015) Influence of fluorescent tag on the motility properties
1178 of kinesin-1 in single-molecule assays. *Biophys J* 108: 1133-1143
1179 Okutachi S, Manoharan GB, Kiriazis A, Laurini C, Catillon M, McCormick F, Yli-Kauhaluoma
1180 J, Abankwa D (2021) A Covalent Calmodulin Inhibitor as a Tool to Study Cellular Mechanisms of K-
1181 Ras-Driven Stemness. *Front Cell Dev Biol* 9: 665673
1182 Olguin HC, Olwin BB (2004) Pax-7 up-regulation inhibits myogenesis and cell cycle
1183 progression in satellite cells: a potential mechanism for self-renewal. *Dev Biol* 275: 375-388
1184 Olson EN, Spizz G, Tainsky MA (1987) The oncogenic forms of N-ras or H-ras prevent skeletal
1185 myoblast differentiation. *Mol Cell Biol* 7: 2104-2111
1186 Pal R, Mamidi MK, Das AK, Bhonde R (2012) Diverse effects of dimethyl sulfoxide (DMSO)
1187 on the differentiation potential of human embryonic stem cells. *Arch Toxicol* 86: 651-661
1188 Parisi B, Sunnen M, Chippalkatti R, Abankwa DK (2023) A flow-cytometry-based pipeline for
1189 the rapid quantification of C2C12 cell differentiation. *STAR Protoc* 4: 102637
1190 Pavic K, Chippalkatti R, Abankwa D (2022) Drug targeting opportunities en route to Ras
1191 nanoclusters. *Adv Cancer Res* 153: 63-99
1192 Post Y, Clevers H (2019) Defining Adult Stem Cell Function at Its Simplest: The Ability to
1193 Replace Lost Cells through Mitosis. *Cell Stem Cell* 25: 174-183
1194 Prior IA, Hood FE, Hartley JL (2020) The Frequency of Ras Mutations in Cancer. *Cancer Res*
1195 80: 2969-2974
1196 Punekar SR, Velcheti V, Neel BG, Wong KK (2022) The current state of the art and future
1197 trends in RAS-targeted cancer therapies. *Nat Rev Clin Oncol* 19: 637-655
1198 Quinlan MP, Quatela SE, Philips MR, Settleman J (2008) Activated Kras, but not Hras or Nras,
1199 may initiate tumors of endodermal origin via stem cell expansion. *Mol Cell Biol* 28: 2659-2674
1200 Rabara D, Tran TH, Dharmaiah S, Stephens RM, McCormick F, Simanshu DK, Holderfield M
1201 (2019) KRAS G13D sensitivity to neurofibromin-mediated GTP hydrolysis. *Proc Natl Acad Sci U S A*
1202 116: 22122-22131
1203 Rauen KA (2013) The RASopathies. *Annu Rev Genomics Hum Genet* 14: 355-369
1204 Rommel C, Clarke BA, Zimmermann S, Nunez L, Rossman R, Reid K, Moelling K,
1205 Yancopoulos GD, Glass DJ (1999) Differentiation stage-specific inhibition of the Raf-MEK-ERK
1206 pathway by Akt. *Science* 286: 1738-1741

1207 Scheffzek K, Ahmadian MR, Kabsch W, Wiesmuller L, Lautwein A, Schmitz F, Wittinghofer
1208 A (1997) The Ras-RasGAP complex: structural basis for GTPase activation and its loss in oncogenic
1209 Ras mutants. *Science* 277: 333-338

1210 Schmick M, Kraemer A, Bastiaens PI (2015) Ras moves to stay in place. *Trends Cell Biol* 25:
1211 190-197

1212 Schubbert S, Zenker M, Rowe SL, Boll S, Klein C, Bollag G, van der Burgt I, Musante L,
1213 Kalscheuer V, Wehner LE *et al* (2006) Germline KRAS mutations cause Noonan syndrome. *Nat Genet*
1214 38: 331-336

1215 She X, Gao Y, Zhao Y, Yin Y, Dong Z (2021) A high-throughput screen identifies inhibitors
1216 of lung cancer stem cells. *Biomed Pharmacother* 140: 111748

1217 Sherman SP, Pyle AD (2013) Small molecule screening with laser cytometry can be used to
1218 identify pro-survival molecules in human embryonic stem cells. *PLoS One* 8: e54948

1219 Shern JF, Chen L, Chmielecki J, Wei JS, Patidar R, Rosenberg M, Ambrogio L, Auclair D,
1220 Wang J, Song YK *et al* (2014) Comprehensive genomic analysis of rhabdomyosarcoma reveals a
1221 landscape of alterations affecting a common genetic axis in fusion-positive and fusion-negative tumors.
1222 *Cancer Discov* 4: 216-231

1223 Shu L, Houghton PJ (2009) The mTORC2 complex regulates terminal differentiation of C2C12
1224 myoblasts. *Mol Cell Biol* 29: 4691-4700

1225 Siddiqui FA, Vukic V, Salminen TA, Abankwa D (2021) Elaiophylin Is a Potent Hsp90/ Cdc37
1226 Protein Interface Inhibitor with K-Ras Nanocluster Selectivity. *Biomolecules* 11

1227 Siljamaki E, Abankwa D (2016) SPRED1 Interferes with K-ras but Not H-ras Membrane
1228 Anchorage and Signaling. *Mol Cell Biol* 36: 2612-2625

1229 Simanshu DK, Nissley DV, McCormick F (2017) RAS Proteins and Their Regulators in Human
1230 Disease. *Cell* 170: 17-33

1231 Skapek SX, Ferrari A, Gupta AA, Lupo PJ, Butler E, Shipley J, Barr FG, Hawkins DS (2019)
1232 Rhabdomyosarcoma. *Nat Rev Dis Primers* 5: 1

1233 Skoulidis F, Li BT, Dy GK, Price TJ, Falchook GS, Wolf J, Italiano A, Schuler M, Borghaei
1234 H, Barlesi F *et al* (2021) Sotorasib for Lung Cancers with KRAS p.G12C Mutation. *N Engl J Med* 384:
1235 2371-2381

1236 Steffen CL, Kaya P, Schaffner-Reckinger E, Abankwa D (2023) Eliminating oncogenic RAS:
1237 back to the future at the drawing board. *Biochem Soc Trans*

1238 Stevenson DA, Allen S, Tidyman WE, Carey JC, Viskochil DH, Stevens A, Hanson H, Sheng
1239 X, Thompson BA, Okumura MJ *et al* (2012) Peripheral muscle weakness in RASopathies. *Muscle*
1240 *Nerve* 46: 394-399

1241 Stevenson DA, Yang FC (2011) The musculoskeletal phenotype of the RASopathies. *Am J Med*
1242 *Genet C Semin Med Genet* 157C: 90-103

1243 Stowe IB, Mercado EL, Stowe TR, Bell EL, Oses-Prieto JA, Hernandez H, Burlingame AL,
1244 McCormick F (2012) A shared molecular mechanism underlies the human rasopathies Legius syndrome
1245 and Neurofibromatosis-1. *Genes Dev* 26: 1421-1426

1246 Tidyman WE, Goodwin AF, Maeda Y, Klein OD, Rauen KA (2022) MEK-inhibitor-mediated
1247 rescue of skeletal myopathy caused by activating Hras mutation in a Costello syndrome mouse model.
1248 *Dis Model Mech* 15

1249 Tsai FD, Lopes MS, Zhou M, Court H, Ponce O, Fiordalisi JJ, Gierut JJ, Cox AD, Haigis KM,
1250 Philips MR (2015) K-Ras4A splice variant is widely expressed in cancer and uses a hybrid membrane-
1251 targeting motif. *Proc Natl Acad Sci U S A* 112: 779-784

1252 Tsherniak A, Vazquez F, Montgomery PG, Weir BA, Kryukov G, Cowley GS, Gill S,
1253 Harrington WF, Pantel S, Krill-Burger JM *et al* (2017) Defining a Cancer Dependency Map. *Cell* 170:
1254 564-576 e516

1255 Vasta JD, Peacock DM, Zheng Q, Walker JA, Zhang Z, Zimprich CA, Thomas MR, Beck MT,
1256 Binkowski BF, Corona CR *et al* (2022) KRAS is vulnerable to reversible switch-II pocket engagement
1257 in cells. *Nat Chem Biol* 18: 596-604

1258 Velica P, Bunce CM (2011) A quick, simple and unbiased method to quantify C2C12 myogenic
1259 differentiation. *Muscle Nerve* 44: 366-370
1260 Wakioka T, Sasaki A, Kato R, Shouda T, Matsumoto A, Miyoshi K, Tsuneoka M, Komiya S,
1261 Baron R, Yoshimura A (2001) Spred is a Sprouty-related suppressor of Ras signalling. *Nature* 412:
1262 647-651
1263 Wall VE, Garvey LA, Mehalko JL, Procter LV, Esposito D (2014) Combinatorial assembly of
1264 clone libraries using site-specific recombination. *Methods Mol Biol* 1116: 193-208
1265 Wang MT, Holderfield M, Galeas J, Delrosario R, To MD, Balmain A, McCormick F (2015)
1266 K-Ras Promotes Tumorigenicity through Suppression of Non-canonical Wnt Signaling. *Cell* 163: 1237-
1267 1251
1268 Wang X, Allen S, Blake JF, Bowcut V, Briere DM, Calinisan A, Dahlke JR, Fell JB, Fischer
1269 JP, Gunn RJ *et al* (2022) Identification of MRTX1133, a Noncovalent, Potent, and Selective
1270 KRAS(G12D) Inhibitor. *J Med Chem* 65: 3123-3133
1271 Weiswald LB, Bellet D, Dangles-Marie V (2015) Spherical cancer models in tumor biology.
1272 *Neoplasia* 17: 1-15
1273 Weyman CM, Wolfman A (1998) Mitogen-activated protein kinase kinase (MEK) activity is
1274 required for inhibition of skeletal muscle differentiation by insulin-like growth factor 1 or fibroblast
1275 growth factor 2. *Endocrinology* 139: 1794-1800
1276 Whyte DB, Kirschmeier P, Hockenberry TN, Nunez-Oliva I, James L, Catino JJ, Bishop WR,
1277 Pai JK (1997) K- and N-Ras are geranylgeranylated in cells treated with farnesyl protein transferase
1278 inhibitors. *J Biol Chem* 272: 14459-14464
1279 Xu Q, Wu Z (2000) The insulin-like growth factor-phosphatidylinositol 3-kinase-Akt signaling
1280 pathway regulates myogenin expression in normal myogenic cells but not in rhabdomyosarcoma-
1281 derived RD cells. *J Biol Chem* 275: 36750-36757
1282 Yablonka-Reuveni Z, Rivera AJ (1994) Temporal expression of regulatory and structural
1283 muscle proteins during myogenesis of satellite cells on isolated adult rat fibers. *Dev Biol* 164: 588-603
1284 Yan W, Markegard E, Dharmaiah S, Urisman A, Drew M, Esposito D, Scheffzek K, Nissley
1285 DV, McCormick F, Simanshu DK (2020) Structural Insights into the SPRED1-Neurofibromin-KRAS
1286 Complex and Disruption of SPRED1-Neurofibromin Interaction by Oncogenic EGFR. *Cell Rep* 32:
1287 107909
1288 Yelland T, Garcia E, Parry C, Kowalczyk D, Wojnowska M, Gohlke A, Zalar M, Cameron K,
1289 Goodwin G, Yu Q *et al* (2022) Stabilization of the RAS:PDE6D Complex Is a Novel Strategy to Inhibit
1290 RAS Signaling. *J Med Chem* 65: 1898-1914
1291 Yin H, Price F, Rudnicki MA (2013) Satellite cells and the muscle stem cell niche. *Physiol Rev*
1292 93: 23-67
1293 Yohe ME, Gryder BE, Shern JF, Song YK, Chou HC, Sindiri S, Mendoza A, Patidar R, Zhang
1294 X, Guha R *et al* (2018) MEK inhibition induces MYOG and remodels super-enhancers in RAS-driven
1295 rhabdomyosarcoma. *Sci Transl Med* 10
1296 Yoon MS (2017) mTOR as a Key Regulator in Maintaining Skeletal Muscle Mass. *Front*
1297 *Physiol* 8: 788
1298 Yoshida N, Yoshida S, Koishi K, Masuda K, Nabeshima Y (1998) Cell heterogeneity upon
1299 myogenic differentiation: down-regulation of MyoD and Myf-5 generates 'reserve cells'. *J Cell Sci* 111
1300 (Pt 6): 769-779
1301 Zembruski NC, Stache V, Haefeli WE, Weiss J (2012) 7-Aminoactinomycin D for apoptosis
1302 staining in flow cytometry. *Anal Biochem* 429: 79-81
1303

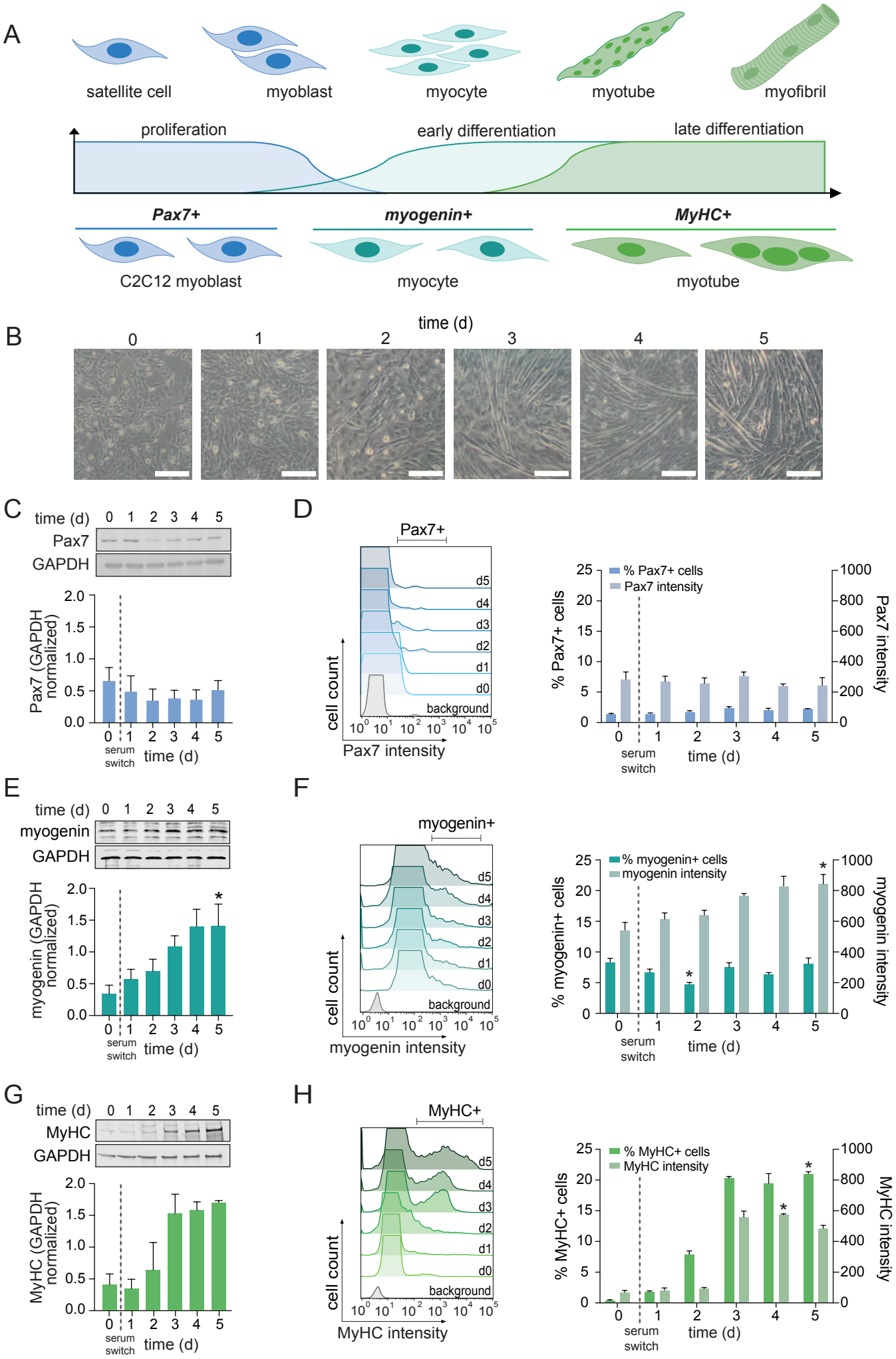
A
satellite cell
myoblast
myocyte
myotube
myofibril
proliferation
early differentiation
late differentiation
Pax7+
myogenin+
MyHC+
C2C12 myoblast
myocyte
myotube
B
time (d)
0
1
2
3
4
5
C
time (d) 0 1 2 3 4 5
Pax7
GAPDH
Pax7 (GAPDH normalized)
serum switch
time (d)
D
Pax7+
d5
d4
d3
d2
d1
d0
background
cell count
Pax7 intensity
% Pax7+ cells
Pax7 intensity
E
time (d) 0 1 2 3 4 5
myogenin
GAPDH
myogenin (GAPDH normalized)
F
myogenin+
% myogenin+ cells
myogenin intensity
G
time (d) 0 1 2 3 4 5
MyHC
GAPDH
MyHC (GAPDH normalized)
H
MyHC+
MyHC intensity
% MyHC+ cells
MyHC intensity

Figure 1

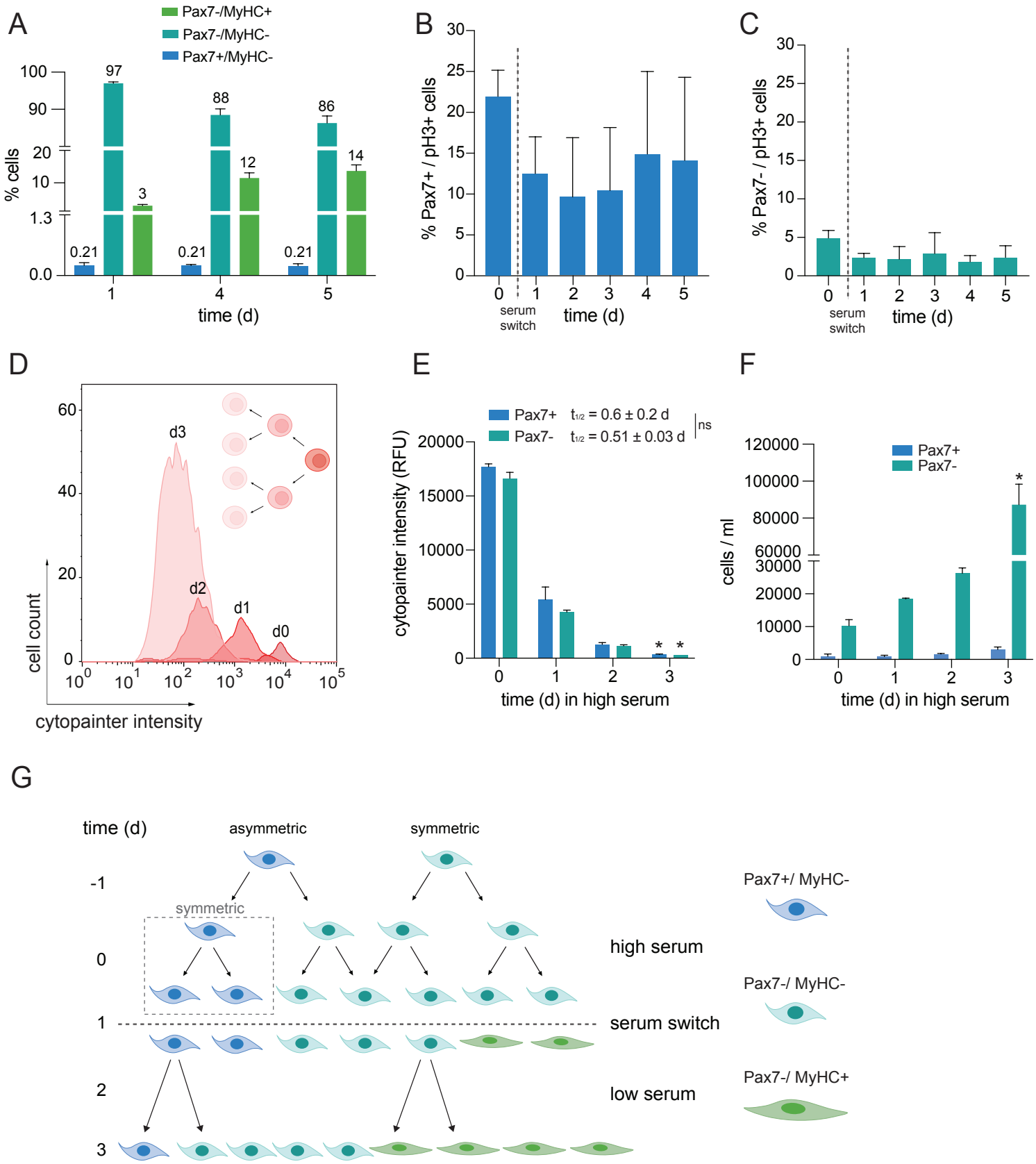
A
Pax7-/MyHC+
Pax7-/MyHC-
Pax7+/MyHC-
% cells
time (d)
B
% Pax7+ / pH3+ cells
serum switch
time (d)
C
% Pax7- / pH3+ cells
serum switch
time (d)
D
cell count
cytopainter intensity
d3
d2
d1
d0
E
Pax7+ t1/2 = 0.6 ± 0.2 d
Pax7- t1/2 = 0.51 ± 0.03 d
ns
cytopainter intensity (RFU)
time (d) in high serum
F
Pax7+
Pax7-
cells / ml
time (d) in high serum
G
time (d)
asymmetric
symmetric
symmetric
high serum
serum switch
low serum
Pax7+/ MyHC-
Pax7-/ MyHC-
Pax7-/ MyHC+

Figure 2

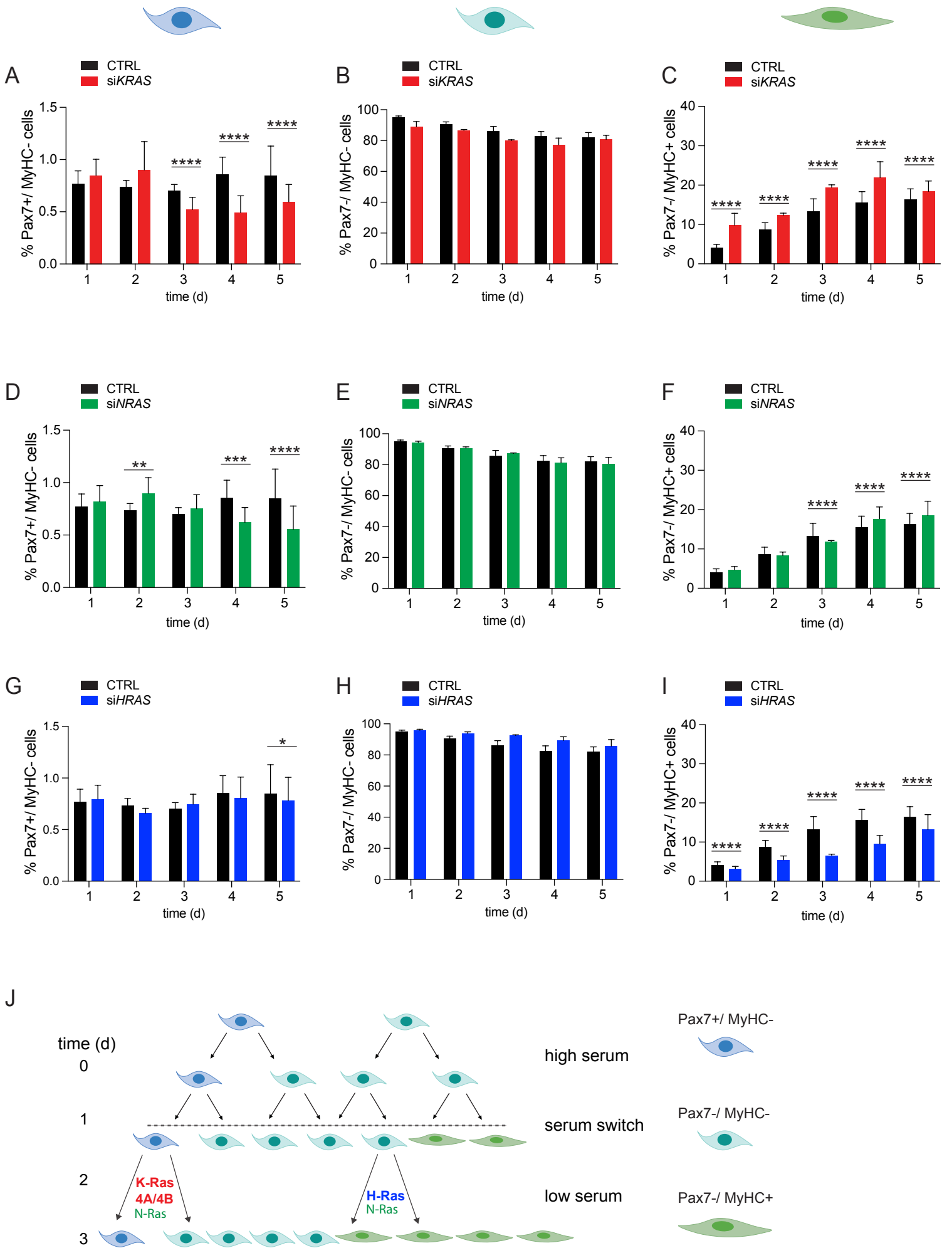
A
CTRL
siKRAS
% Pax7+/ MyHC- cells
time (d)
B
% Pax7-/ MyHC- cells
C
% Pax7-/ MyHC+ cells
D
siNRAS
E
F
G
siHRAS
H
I
J
time (d)
0
1
2
3
high serum
serum switch
low serum
K-Ras
4A/4B
N-Ras
H-Ras
N-Ras
Pax7+/ MyHC-
Pax7-/ MyHC-
Pax7-/ MyHC+

Figure 3

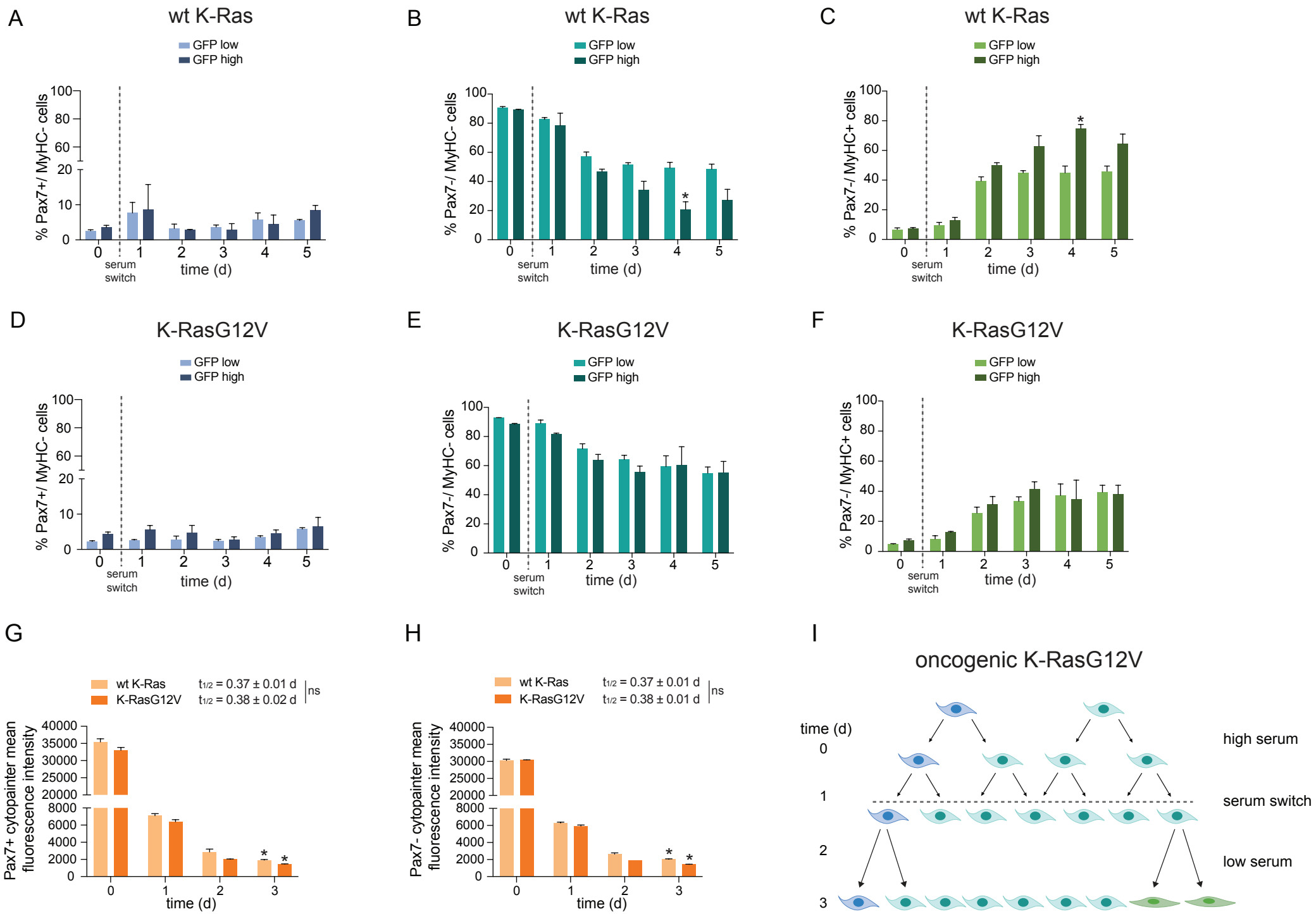
A
wt K-Ras
GFP low
GFP high
% Pax7+/ MyHC- cells
serum switch
time (d)
B
wt K-Ras
GFP low
GFP high
% Pax7-/ MyHC- cells
serum switch
time (d)
C
wt K-Ras
GFP low
GFP high
% Pax7-/ MyHC+ cells
serum switch
time (d)
D
K-RasG12V
GFP low
GFP high
% Pax7+/ MyHC- cells
serum switch
time (d)
E
K-RasG12V
GFP low
GFP high
% Pax7-/ MyHC- cells
serum switch
time (d)
F
K-RasG12V
GFP low
GFP high
% Pax7-/ MyHC+ cells
serum switch
time (d)
G
wt K-Ras t1/2 = 0.37 ± 0.01 d
K-RasG12V t1/2 = 0.38 ± 0.02 d
ns
Pax7+ cytopainter mean fluorescence intensity
time (d)
H
wt K-Ras t1/2 = 0.37 ± 0.01 d
K-RasG12V t1/2 = 0.38 ± 0.01 d
ns
Pax7- cytopainter mean fluorescence intensity
time (d)
I
oncogenic K-RasG12V
time (d)
high serum
serum switch
low serum

Figure 4

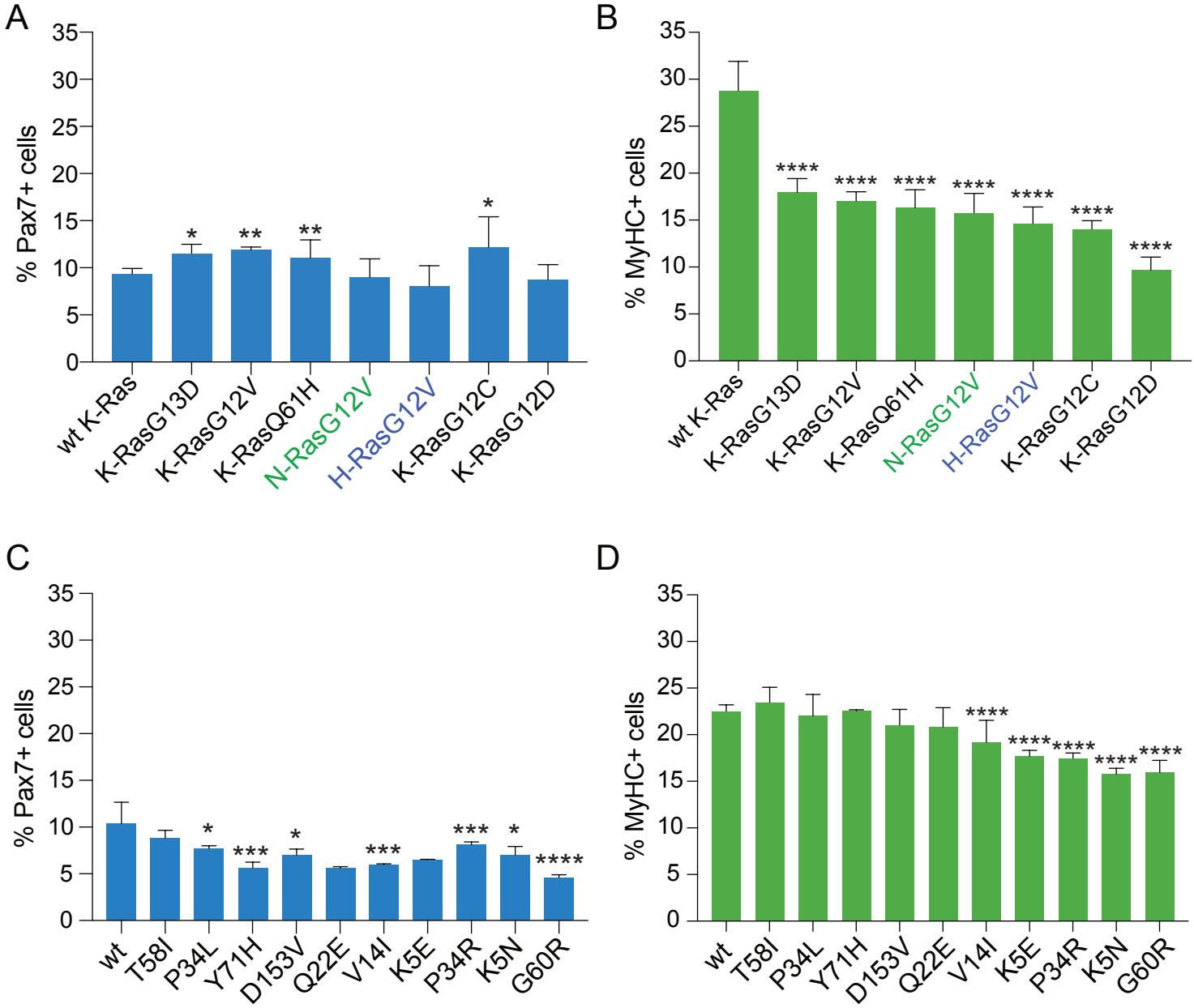
A
% Pax7+ cells
35
30
25
20
15
10
5
0
*
**
**
*
wt K-Ras
K-RasG13D
K-RasG12V
K-RasQ61H
N-RasG12V
H-RasG12V
K-RasG12C
K-RasG12D
B
% MyHC+ cells
****
C
% Pax7+ cells
***
****
wt
T58I
P34L
Y71H
D153V
Q22E
V14I
K5E
P34R
K5N
G60R
D
% MyHC+ cells

Figure 5

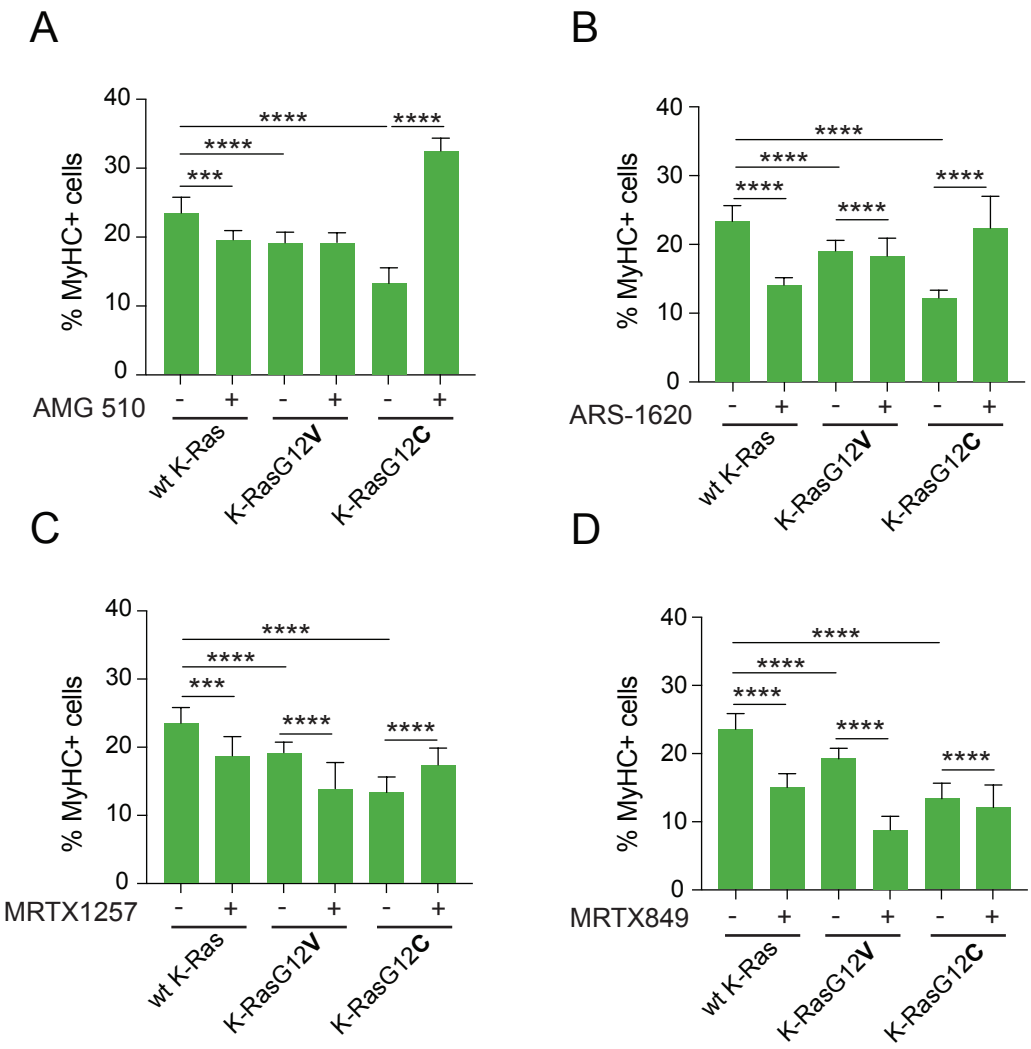
A
% MyHC+ cells
40
30
20
10
0
****
****
***
****
AMG 510
- + - + - +
wt K-Ras
K-RasG12V
K-RasG12C
B
% MyHC+ cells
40
30
20
10
0
****
****
****
****
****
ARS-1620
- + - + - +
wt K-Ras
K-RasG12V
K-RasG12C
C
% MyHC+ cells
40
30
20
10
0
****
****
***
****
****
MRTX1257
- + - + - +
wt K-Ras
K-RasG12V
K-RasG12C
D
% MyHC+ cells
40
30
20
10
0
****
****
****
****
****
MRTX849
- + - + - +
wt K-Ras
K-RasG12V
K-RasG12C

Figure 6

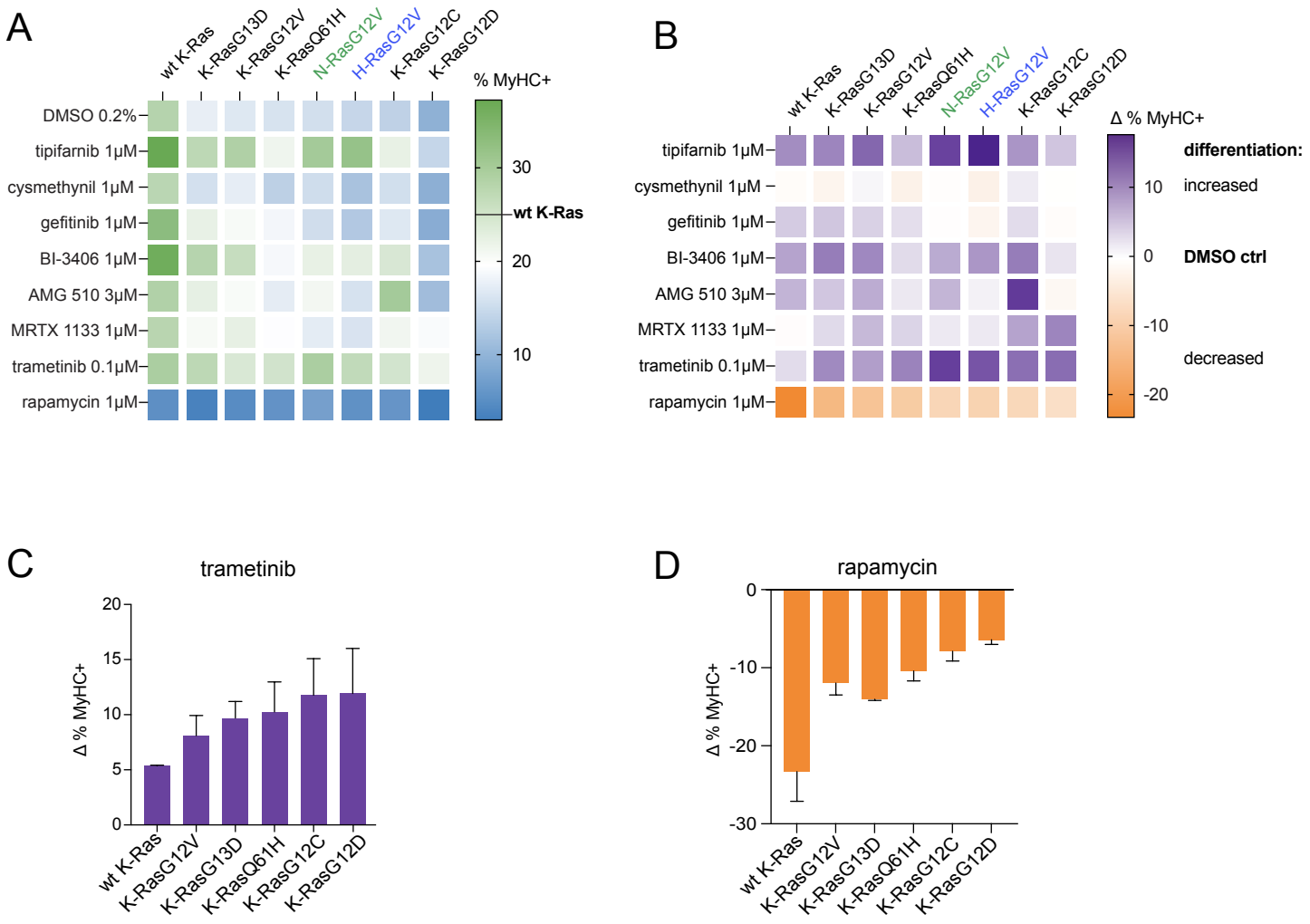
A
wt K-Ras
K-RasG13D
K-RasG12V
K-RasQ61H
N-RasG12V
H-RasG12V
K-RasG12C
K-RasG12D
% MyHC+
DMSO 0.2%
tipifarnib 1μM
cysmethynil 1μM
gefitinib 1μM
BI-3406 1μM
AMG 510 3μM
MRTX 1133 1μM
trametinib 0.1μM
rapamycin 1μM
30
wt K-Ras
20
10
B
Δ % MyHC+
differentiation:
increased
DMSO ctrl
decreased
10
0
-10
-20
C
trametinib
Δ % MyHC+
20
15
10
5
0
D
rapamycin
0
-10
-20
-30

Figure 7